Neurobiology of Disease 132 (2019) 104561

Contents lists available at ScienceDirect

Neurobiology of Disease

journal homepage: www.elsevier.com/locate/ynbdi

Stem cell factor and granulocyte colony-stimulating factor promote brain repair and improve cognitive function through VEGF-A in a mouse model of CADASIL

Suning Ping, Xuecheng Qiu, Michele Kyle, Karen Hughes, John Longo, Li-Ru Zhao*

Department of Neurosurgery, State University of New York Upstate Medical University, Syracuse, NY 13210, USA

ARTICLE INFO

Keywords:
CADASIL
SCF
G-CSF
VEGF
VEGF-A

ABSTRACT

Cerebral autosomal dominant arteriopathy with subcortical infarct and leukoencephalopathy (CADASIL) is a cerebral small vascular disease caused by NOTCH3 gene mutation in vascular smooth muscle cells (VSMCs), leading to ischemic stroke and vascular dementia. To date, the pathogenesis of CADASIL remains poorly understood, and there is no treatment that can slow the progression of CADASIL. Using a transgenic mouse model of CADASIL (TgNotch3R90C), this study reveals novel findings for understanding CADASIL pathogenesis that decreased cerebral vascular endothelial growth factor (VEGF/VEGF-A) is linked to reduced cerebral blood vessel density. Reduced endothelial cell (EC) proliferation and angiogenesis are seen in TgNotch3R90C mouse brain-isolated ECs. Decreased dendrites, axons, and synapses in the somatosensory and motor cortex layer 2/3 and in the hippocampal CA1, and reduced neurogenesis in both the subventricular zone and subgranular zone occur in 15-month-old TgNotch3R90C mice. These reductions in neuron structures, synapses, and neurogenesis are significantly correlated to decreased cerebral vasculature in the corresponding areas. Impaired spatial learning and memory in TgNotch3R90C mice are significantly correlated with the reduced cerebral vasculature, neuron structures, and synapses. Repeated treatment of stem cell factor and granulocyte colony-stimulating factor (SCF + G-CSF) at 9 and 10 months of age improves cognitive function, increases cerebral VEGF/VEGF-A, restores cerebral vasculature, and enhances regeneration of neuronal structures, synaptogenesis and neurogenesis in TgNotch3R90C mice. Pretreatment with Avastin, an angiogenesis inhibitor by neutralizing VEGF-A, completely eliminates the SCF + G-CSF-enhanced cognitive function, vascular and neuronal structure regeneration, synaptogenesis and neurogenesis in TgNotch3R90C mice. SCF + G-CSF-enhanced EC proliferation and angiogenesis in TgNotch3R90C mouse brain-isolated ECs are also blocked by Avastin pretreatment. These data suggest that SCF + G-CSF treatment may repair Notch3R90C mutation-damaged brain through the VEGF-A-mediated angiogenesis. This study provides novel insight into the involvement of VEGF/VEGF-A in the pathogenesis of CADASIL and sheds light on the mechanism underlying the SCF + G-CSF-enhanced brain repair in CADASIL.

1. Introduction

Cerebral autosomal dominant arteriopathy with subcortical infarct and leukoencephalopathy (CADASIL) is the common monogenic cause of cerebral small vascular disease, and represents the most frequent form of hereditary ischemic stroke and vascular dementia in adults (Chabriat et al., 2009). CADASIL mainly affects young and middle-aged adults, and causes severe disability and early death (Chabriat et al., 1995; Peters et al., 2004a,b; Joutel, 2011; Di Donato et al., 2017). It has long been thought that CADASIL is a rare genetic disease. However, a recent genetic study challenges this notion. The prevalence of CADASIL mutations is 3.4/1000 in the world, which is 100 times higher than previously thought (Rutten et al., 2016). Up to now, the pathogenesis of CADASIL remains poorly understood, and there is no treatment that can

Abbreviations: CADASIL, Cerebral autosomal dominant arteriopathy with subcortical infarct and leukoencephalopathy; VSMC, Vascular smooth muscle cell; VEGF, Vascular endothelial growth factor; SCF, Stem cell factor; G-CSF, Granulocyte colony-stimulating factor; CNS, Central nervous system; WT, Wild type; PBS, Phosphate buffered saline; BSA, Bovine serum albumin; MAP2, Microtubule associated protein 2; SMI312, Pan-axonal neurofilament marker; DCX, Doublecortin; PSD-95, Postsynaptic density protein 95; ANOVA, Analysis of variance; SVZ, Subventricular zone; SGZ, Subgranular zone; EGFR, Epidermal growth factor-like repeat; EC, Endothelial cell

* Corresponding author at: Department of Neurosurgery, State University of New York Upstate Medical University, 750 E. Adams Street, Syracuse, NY 13210, USA.
E-mail address: ZHAOL@upstate.edu (L.-R. Zhao).

https://doi.org/10.1016/j.nbd.2019.104561
Received 3 January 2019; Received in revised form 28 June 2019; Accepted 30 July 2019
Available online 31 July 2019
0969-9961/ Published by Elsevier Inc.

stop or even delay the progression of CADASIL.

NOTCH3 gene mutation is the cause of this genetic disease (Joutel et al., 1996). The Notch3 receptor encoded by NOTCH3 gene is predominantly expressed in the vascular smooth muscle cells (VSMCs) of small arteries (Joutel et al., 2000; Villa et al., 2001) and in the pericytes of capillaries (Joutel et al., 2010). NOTCH3 mutation may cause defective vascular function in the vascular system; however, the symptoms of CADASIL are almost exclusively restricted to the brain (Joutel et al., 2010). Accumulating studies in both CADASIL patients (Baudrimont et al., 1993; Chabriat et al., 1995; Kalimo et al., 1999; Chabriat et al., 2000; Miao et al., 2004; Tuominen et al., 2004; Miao et al., 2006; De Guio et al., 2014) and mouse models (Ruchoux et al., 2003; Dubroca et al., 2005; Lacombe et al., 2005; Joutel et al., 2010; Gu et al., 2012; Liu et al., 2015) have revealed degeneration and loss of VSMCs in small arteries and capillary pericytes in the brain, cerebrovascular dysfunction, decreased cerebrovascular density, and reduced cerebral blood flow.

Stem cell factor (SCF) and granulocyte colony-stimulating factor (G-CSF) are the essential hematopoietic growth factors and play key roles in regulating blood cell production and bone marrow stem cell survival and mobilization (Welte et al., 1985; Zsebo et al., 1990). In addition to their biological function in the hematopoietic system, SCF and G-CSF also play roles in pathological conditions in the central nervous system (CNS). It has been demonstrated that decreased plasma levels of SCF and G-CSF are tightly linked to the severity of Alzheimer's disease (Laske et al., 2008, 2009). Administration of SCF and G-CSF has been shown to improve functional recovery in animal models of stroke (Kawada et al., 2006; Zhao et al., 2007). SCF in combination with G-CSF (SCF + G-CSF) treatment in the chronic phase of experimental stroke enhances angiogenesis and neural network regrowth, and improves functional recovery (Cui et al., 2015, 2016). Our earlier study has demonstrated that SCF + G-CSF treatment not only reduces VSMC degeneration, but it also increases blood vessel density and improves cognitive function in a transgenic mouse model of CADASIL (TgNothch3R90C) (Liu et al., 2015). Emerging evidence has revealed a positive link between cerebrovascular density and brain health (Williamson et al., 2018). It remains unclear, however, how SCF + G-CSF treatment enhances angiogenesis and whether the enhanced cerebral vessel density is required for SCF + G-CSF-improved cognitive function in a CADASIL condition.

Neurovascular coupling is essential to ensure proper function in the brain (Phillips et al., 2016). The brain possesses a highly specialized vasculature to meet the demands of highly active metabolism in the brain and to protect the neurons from toxicity of metabolic wastes (Venkat et al., 2016). In adults, the brain is predominantly vascularized through the process of angiogenesis (Shibuya, 2009). Many molecular mechanisms underlying angiogenesis in the adult brain have been identified, while the vascular endothelial growth factor (VEGF) has been proven to be the most potent proangiogenic factor (Vallon et al., 2014).

Using the TgNothch3R90C transgenic mouse model of CADASIL, this study aims to determine whether VEGF is involved in SCF + G-CSF-enhanced angiogenesis and whether the increased angiogenesis is a key driver for brain repair and cognitive improvement by SCF + G-CSF treatment.

2. Materials and methods

The experimental procedures were conducted in accordance with the guidelines of National Institutes of Health. The research protocol of this study was approved by the Institutional Animal Care and Use Committee.

2.1. Animals and experiment design

Transgenic mice carrying a full-length human NOTCH3 gene with the Arginine-to-Cysteine (Arg90Cys) mutation at amino acid position 90 driven by the SM22α promoter in VSMCs were used as a mouse model of CADASIL (Ruchoux et al., 2003; Monet-Lepretre et al., 2009) (TgNotch3R90C). The original breeders were generously provided as gifts from Dr. Anne Joutel (Faculté de Médecine, Paris, France). Mice were housed in polycarbonate cages (2-5mice/cage) on an artificial 12-h light-12h dark cycle with *ad libitum* access to water and a standard laboratory diet. Nine-month-old male TgNotch3R90C mice were randomly divided into four groups (n = 11–17/group): a vehicle control group, an Avastin treatment group, an SCF + G-CSF treatment group, and a group treated with both Avastin and SCF + G-CSF. Age-matched wild type (WT) mice were used as WT controls. The first treatment was performed at 9 months of age. Recombinant mouse SCF (PeproTech) and recombinant human G-CSF (Amgen) (SCF: 200 μg/kg, diluted in saline; G-CSF: 50 μg/kg, diluted in 5% dextrose) or an equal volume of vehicle solution (50% of saline and 50% of 5% dextrose) was subcutaneously injected for seven consecutive days. To block the VEGF-A-mediated angiogenesis, Avastin (Bevacizumab) (Roche) (15 mg/kg, i.p.) was administered 1 h before SCF + G-CSF treatment. The same treatment was repeated again at the age of 10 months. Twenty-four hours after the final treatment at 10 months of age, three mice were randomly chosen from each group to assess the levels of VEGF in the brain through Western Blot. Seven weeks after completion of the second treatment paradigm (equal to 12 months of age), water maze test was performed in the remaining mice (n = 8–14/group) to evaluate spatial learning and memory. At the age of 15 months, mice were euthanized to examine structural changes in the brain by immunohistochemistry (n = 7-11/group, due to loss of some mice by the end of experiment) (see experimental flowchart in Fig. 1).

2.2. Water maze test

During the water maze testing, the performance for each mouse was recorded and tracked by an ANY-Maze video system.

The water maze test was utilized to evaluate spatial learning and memory. A four-foot diameter water tank was filled with water (22 °C) mixed with non-toxic white paint. A cylindrical platform was hidden 1 cm beneath the surface of water and fixed in the position aligned with schematic area on the computer. The water maze test was performed daily for a total of five days. Each day included four swimming trials (1 min/trial) starting randomly from each of the four starting positions. On the first day of the trial, mice were guided to and remained on the platform for 15 s after the 1-min testing period was completed. After completing the test, mice were removed from the water, wiped off with paper towels and warmed up in the cage with a heating pad.

2.3. Immunohistochemistry and histochemistry

After being anesthetized, mice were transcardially perfused with phosphate buffered saline (PBS) containing heparin (10 U/ml, Sagent

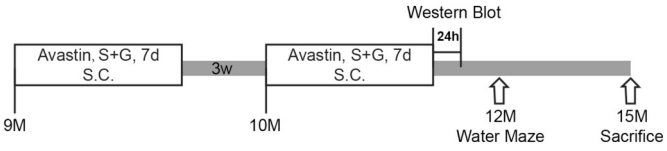

Fig. 1. Schematic flowchart of the experiment. Nine-month-old TgNotch3R90C mice were injected with Avastin (intraperitoneally, i.p.) and/or SCF + G-CSF (subcutaneously, s.c.) for seven consecutive days. An equal volume of vehicle solution was injected in the control TgNotch3R90C mice. The same treatment was repeatedly administered three weeks later at the age of 10 months. Three mice were randomly chosen from each group and euthanized 24 h after the final injection for Western Blot analysis. A water maze test was performed in the remaining mice at 12 months of age. Mice were sacrificed for immunohistochemistry at the age of 15 months.

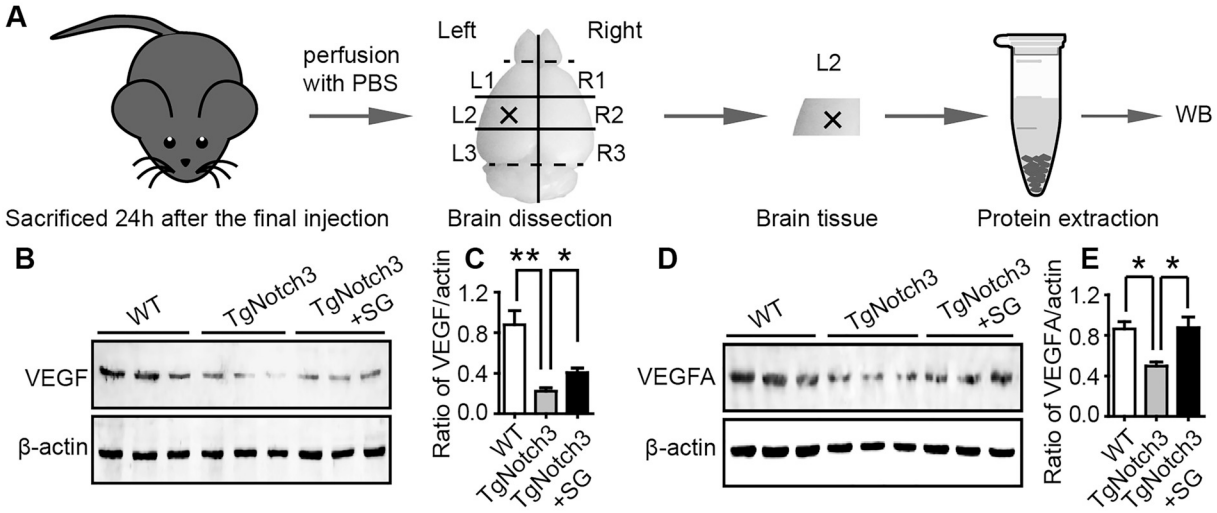

Fig. 2. Cerebral protein levels of VEGF and VEGF-A by Western Blotting. Note that reduced VEGF and VEGF-A production in the brains of TgNotch3R90C mice are elevated by SCF + G-CSF treatment. (A) A schematic diagram shows brain tissue collection for Western Blotting. The brain was isolated after PBS perfusion and cut coronally into three parts. Brain tissue from the middle part was further divided into two parts. The brain tissue of the left hemisphere was used for experiment. (B-E) Western blot data. The levels of VEGF (B and C) and VEGF-A (D and E) in the brains of TgNotch3R90C mice and age-matched wild type (WT) control mice. Mean ± S.E.M. $N = 3$. *p < .05, **p < .01. One-way ANOVA with Tukey *post hoc* test.

Pharmaceuticals) followed by 10% neutral buffered formalin (Sigma) perfusion. Brains were removed, post-fixed in the same fixative solution overnight at 4 °C, and then placed in 30% sucrose solution in PBS for two days. After being fully dehydrated, the brains were embedded into O.C.T. compound (Thermo Fisher Scientific) on dry ice. The brains were sectioned at a thickness of 30 μm using a cryostat. Four brain sections per mouse (two sections selected between bregma +0.26 to +0.86 mm and other two sections between bregma −1.46 to −1.94 mm) were used for the immunohistochemistry. Briefly, brain sections were rinsed with PBS. Nonspecific binding was blocked with 10% donkey serum in 1% bovine serum albumin (BSA) (IgG free, Jackson Immunoresearch) and 0.3% Triton X-100 solution (Sigma) for 1 h at room temperature. Brain sections were also blocked with mouse on mouse blocking reagent (M.O.M.™) (Vector Laboratories) for 1 h at room temperature before staining with mouse-derived primary antibodies. Sections were then incubated with primary antibodies overnight at 4 °C. The primary antibodies used in this study were microtubule associated protein 2 (MAP2) (1:600, rabbit, Chemicon), pan-axonal neurofilament marker (SMI312) (1:1000, mouse, Biolegend), doublecortin (DCX) (1:200, goat, Santa Cruz), synaptophysin (1:1000, rabbit, Sigma), and VEGF (1:1000, rabbit, Thermo Fisher Scientific). The following day, after being washed with PBS, brain sections were incubated with the appropriate secondary antibody for 2 h at room temperature in the dark. Secondary antibodies used were Alexa Fluor 594-conjugated donkey anti-rabbit, Alexa Fluor 488-conjugated donkey anti-mouse, Alexa Fluor 488-conjugated donkey anti-rabbit, Alexa Fluor 594-conjugated donkey anti-mouse, and Alexa Fluor 594-conjugated donkey anti-goat (Thermo Fisher Scientific). To visualize the brain vessels, sections were incubated with Dylight 488-labeled *Lycopersicon esculentum* (Tomato) Lectin (1:1000, Vector) for 2 h at room temperature. Sections were counterstained with DAPI and mounted with Vectashield antifade mounting medium (Vector Laboratories). The immunofluorescence staining was imaged using a confocal microscope (Zeiss LSM780). Data was analyzed by using ImageJ software.

2.4. Quantitative image analysis

To quantify the percentage of positive area of Lectin staining, brain sections were imaged by the Zeiss LSM 780 confocal microscope under a 10× objective lens using a tile scan (14 × 9). Brain sections were selected between bregma +0.26 to +0.86 mm. Two fields (1050 × 850 μm^2/field) in the cortex and one field (1300 × 1300 μm^2) in the striatum were scanned for each section in the bilateral hemispheres. To quantify the percentage of Lectin positive area in the cortical layer 2–3, two fields (400 × 400 μm^2/field) per section in bilateral cortical layer 2–3 were selected for imaging. In brain sections selected between bregma −1.46 to −1.94 mm, one field (1600 × 850 μm^2) in the hippocampus was imaged for each section in the bilateral hemispheres. To quantify the percentage of Lectin positive area in the hippocampal CA1, two fields (400 × 400 μm^2/field) per section in bilateral hippocampal CA1 were selected for imaging. The percentage of positive areas were measured by ImageJ (NIH software).

Neuronal network density was determined through analyzing MAP2 and SMI312 positive staining. After immunohistochemistry, brain sections were imaged by the Zeiss LSM 780 confocal microscope under the 40× objective lens. Two fields (200 × 400 μm^2/field) in the cortical layer 2–3 and two fields (100 × 180 μm^2/field) in the hippocampal CA1 region were scanned for each section in both hemispheres. The percentage of MAP2 and SMI312 positive areas were measured by ImageJ.

Synaptic density was examined through analyzing SYN immunopositive staining. After immunofluorescence staining, brain sections were imaged by the Zeiss LSM 780 confocal microscope under the 40× objective lens. Two fields (100 × 100 μm^2/field) in the cortical layer 2–3 and hippocampal CA1 for each section were selected for imaging in the bilateral hemispheres. The percentage of SYN positive area and number of SYN positive puncta were measured by ImageJ.

DCX, a marker for neuronal precursor cells and immature neurons, was used for evaluating neurogenesis. The DCX positive cells in the subventricular zone (SVZ) and dentate gyrus (DG) were analyzed. The total DCX positive areas in both hemispheres were measured and normalized by the perimeter of the SVZ. The number of DCX positive cells in the DG was blindly counted and used for statistical analysis.

2.5. Western blot analysis

The brain was removed after PBS perfusion. The olfactory bulb and cerebellum were discarded, and the remaining brain was then cut coronally into three parts. The brain tissue from the middle part was further divided into two parts (the left hemisphere and right hemisphere). The left hemisphere was selected and lysed for protein extraction (see the flowchart in Fig. 2A). The brain tissue was lysed in ice-cold lysis buffer (20 mM sodium phosphate, 5 mM EDTA, 150 mM NaCl,

50 mM NaF and 1% Triton X-100) with inhibitor cocktails (proteinase inhibitor cocktail and phosphatase inhibitor cocktail) (Sigma) according to a certain proportion (1 ml lysis buffer for 20 mg brain tissues). The brain was then minced into small pieces and processed by ultrasonic lysis three times for 1 min each in ice. For the cultured VSMCs, the culture medium was discarded, and the cells were washed with PBS. The VSMCs were then scraped, lysed with the same lysis buffer used for brain tissue for 30 min, and vortexed every 5 min.

The brain tissue lysates and cultured cell lysates were centrifuged, and protein concentration was measured by Bradford assay. Heat-denatured proteins were electrophoresed by SDS-PAGE and transferred to nitrocellulose membranes (Bio-rad). The membranes were blocked with 5% non-fat milk for 1 h at room temperature and then incubated with rabbit anti-mouse VEGF primary antibody (1:1000, Thermo Fisher Scientific) and rat anti-mouse VEGF-A primary antibody (1:1000, Biolegend) overnight at 4 °C. A mouse anti- β-actin (1:1000, Sigma) was used as an internal control. The following day, after being rinsed with 1 × Tris-buffered saline (Bio-rad) with 0.1% Tween 20 (Sigma), the membranes were further incubated with secondary antibodies of alkine phosphatase-conjugated goat anti-rabbit, goat anti-rat, and goat anti-mouse (1:10,000, Sigma) for 2 h at room temperature. The bands were visualized by ECF substrate (Sigma) and scanned with a Chemidoc system. Western Blot data were semi-quantified and analyzed by ImageJ software.

2.6. Primary culture and purification identification of brain-derived endothelial cells

Culturing of primary cerebral endothelial cells (ECs) was carried out by a modification of previous studies (Navone et al., 2013; Ruck et al., 2014). Briefly, brains were removed from 3-month-old male WT and TgNotch3R90C mice and minced into small pieces. After enzymatic digestion with 0.05% collagenase/dispase (Sigma) for 15 min at 37 °C, an equal volume of DMEM containing 10% FBS (Thermo Fisher Scientific) was added to the digested tissues to neutralize the enzymatic digestion. Brain tissues were then triturated with a 10-ml pipette 10 times before centrifuging. After the supernatant was discarded, the tissue pellet was centrifuged in 20% BSA (Boston Bioproducts) diluted with DMEM medium (Thermo Fisher Scientific) to isolate the cerebral vessels. After centrifuging, the supernatant and fatty layer were removed by vacuum, and the cerebral vessel pellet was washed with PBS (Thermo Fisher Scientific). The suspensions were filtered through a 70 μm-mesh filter, and the flow-through was collected in a 50-ml conical tube. The collected tissues in the tube were further digested in 0.05% collagenase/dispase for 30 min at 37 °C in a water bath. An equal volume of DMEM containing 10% FBS was added to the digested tissues to neutralize the enzymatic digestion. After being centrifuged and washed with PBS, the cell pellets were resuspended, seeded on six-well-plates pre-coated with collagen (BD biosciences) and cultured with endothelial cell culture medium containing DMEM, 10% FBS, basic fibroblast growth factor (20 μg/ml) (Thermo Fisher Scientific), heparin (100 μg/ml) (Sagent Pharmaceuticals), and puromycin (4 mg/ml) (Sigma) at 37 °C in a humidified incubator with 5% CO_2. Medium was replaced every three days. Cultured ECs within three passages (< P3) were used for the study.

Cultured ECs at passage one were used for identifying EC purification. Cells were seeded onto collagen pre-coated 24-well-plates at 5×10^4 cells/well. After reaching 80% confluence, cells were fixed with 10% neutral buffered formalin for 10 min at room temperature and washed with PBS. After incubation with 10% donkey serum in 1% BSA and 0.3% Triton X-100 solution for 1 h at room temperature, cells were incubated with a rat anti-mouse CD31 primary antibody (1:300, BD Biosciences) overnight at 4 °C. Thereafter, cells were incubated with a Dylight 594-conjugated donkey anti-rat secondary antibody (Thermo Fisher Scientific) for 2 h at room temperature. After being counterstained with DAPI, cells were mounted with antifade mounting medium (Vectashield, Vector Laboratories). Images were taken by an inverted fluorescent microscope (Zeiss Axio). The number of CD31 positive ECs was blindly counted, and the percentage of CD31 positive ECs in total cells were calculated to assess EC purification.

2.7. Endothelial cell proliferation assay

To determine cerebral EC proliferation, bromodeoxyuridine (BrdU) and Ki-67 immunocytochemistry were performed in the cultured brain-isolated ECs. BrdU, an analog of thymidine, is incorporated into the newly synthesized DNA of proliferating cells during the S phase of cell cycle. Ki-67 protein is a strictly cellular marker for proliferation. Ki-67 is present at all active phases of the cell cycle (G1, S, G2) and mitosis, but is absent in resting cells (G0). Primary cultured cerebral ECs were seeded onto collagen pre-coated 24-well plates at 5×10^4 cells/well. After growth for 24 h, SCF and G-CSF (20 ng/ml) were added to the ECs and incubated for 24 h. To examine the effects of Avastin (Genentech, Roche) on ECs proliferation, Avastin (1 mg/ml) was used to pretreat the cells 1 h prior to the SCF + G-CSF treatment. To label the proliferating ECs at the S phase, BrdU (10 ng/ml, Sigma) was added to the cultured ECs for the last 6 h before collection. The ECs were then fixed with 10% neutral buffered formalin for 10 min at room temperature, treated with 2 N HCl for 30 min at 37 °C, and then rinsed with PBS three times. To detect the active phases of cell cycle, the Ki-67 antibody was used for immunocytochemistry. Briefly, after ECs were fixed with 10% neutral buffered formalin for 10 min at room temperature, nonspecific binding was blocked with 10% donkey serum in 1% BSA and 0.3% Triton X-100 solution for 1 h at room temperature. ECs were also blocked with mouse on mouse blocking reagent (M.O.M.™) for 1 h at room temperature to avoid nonspecific binding from the mouse-derived antibody. Thereafter, the ECs were incubated with mouse anti-BrdU (1:300, Roche Diagnostics Corporation) and rabbit anti-Ki67 (1:500, Thermo Fisher Scientific) overnight at 4 °C. After being washed with PBS, the ECs were incubated with secondary antibodies including Alexa 594-conjugated donkey anti-mouse IgG and Alexa 488-conjugated donkey anti-rabbit IgG (1:500, Thermo Fisher Scientific). Cells were counterstained with DAPI and mounted with Vectashield antifade mounting medium. The immunofluorescence staining was imaged using an inverted fluorescent microscope (Zeiss Axio). Four to six fields were randomly selected in each well for imaging. BrdU and Ki-67 positive cells were quantified by using ImageJ software. The percentage of $BrdU^+$ and $Ki\text{-}67^+$ cells per field was used for statistical analysis.

2.8. Tube formation assay

A tube formation assay was used to determine angiogenesis. The tube formation assay was performed in primary cultured cerebral ECs (< P3). ECs were seeded in Matrigel (200 μl) (BD biosciences) in pre-coated 48-well-plates at 3×10^4 cells/well and treated with or without SCF + G-CSF (20 ng/ml). After six hours growth, cells were fixed with 10% neutral buffered formalin for 10 min at room temperature. To test the role of Avastin on SCF + G-CSF-regulated EC angiogenesis, ECs were pretreated with Avastin (1 mg/ml) 1 h prior to the SCF + G-CSF treatment. Images were taken by an inverted light microscope (Olympus IX73). Tube-like structures in each well were randomly selected 3–6 fields for imaging. The number of branches and total length of branches were calculated by ImageJ.

2.9. Angiogenesis assessment in vivo

To assess the cerebral endothelial cell proliferation in the process of angiogenesis, BrdU was administered to TgNotch3R90C mice with/without SCF + G-CSF treatment. At the age of 18 months, SCF + G-CSF (SCF, 200 μg/kg; G-CSF, 50 μg/kg) or an equal volume of vehicle solution was subcutaneously injected for five consecutive days. BrdU (50 mg/kg, Sigma) was intraperitoneally injected at the last two days

during the 5-day-SCF + G-CSF treatment. On the fourth day of SCF + G-CSF treatment, BrdU was injected twice a day with a 4-h interval initiated at 4 h post-SCF + G-CSF injection. On the last day of SCF + G-CSF treatment, BrdU was injected three times with 4-h intervals. Mice were sacrificed within 24 h after the final injection of BrdU. A chart for the experimental design is shown in Fig. 5.

The procedures of tissue preparation were exactly as the same as described earlier. Four brain sections per mouse (between bregma +0.26 to −1.94 mm) were used for immunohistochemistry. Brain sections were treated with 2 N HCl for 1 h at room temperature. Nonspecific binding was blocked with 10% donkey serum in 1% BSA and 0.3% TritonX-100 solution for 1 h at room temperature. Brain sections were also incubated with mouse on mouse blocking reagent (M.O.M.™) (Vector Laboratories) for 1 h at room temperature. Sections were then incubated with rabbit anti-CD31 (1:50, Abcam) and mouse anti-BrdU (1:500, Roche) overnight at 4 °C. After being washed with PBS, brain sections were incubated with Alexa Fluor 594-conjugated donkey anti-rabbit and Alexa Fluor 488-conjugated donkey anti-mouse for 2 h at room temperature in the dark. Sections were counterstained with DAPI and mounted with Vectashield antifade mounting medium (Vector Laboratories). The immunofluorescence staining was imaged with the Zeiss LSM780 confocal microscope under a 40× objective lens using a *Z*-stack scan. The images were analyzed with ImageJ software, and the number of $BrdU^+CD31^+$ cells in each brain section was qualified.

2.10. Statistics

Data collection and analysis were carried out by using randomization and blind approaches. Depending on the distribution of the data, parametric statistics were carried out by one-way or repeated two-way analysis of variance (ANOVA) followed by Tukey *post hoc* multiple comparison test, and nonparametric test was performed by Kruskal-Wallis analysis with Dunn's multiple comparison test. The unpaired *t*-test was used for the comparison between two independent groups. Correlation tests were calculated using linear regression. Results were considered significant differences when a p value was < 0.05. Data were presented as mean ± S.E.M.. Statistical analysis was performed using Graphpad Prism (GraphPad Software, Inc., La Jolla, CA, USA).

3. Results

3.1. Reduced VEGF production in the brains of TgNotch3R90C mice is elevated by SCF + G-CSF treatment

In our previous study, we demonstrated that decreased blood vessel density in the brain of TgNotch3R90C mice is restored by SCF + G-CSF treatment (Liu et al., 2015). However, the mechanism underlying the SCF + G-CSF-restored cerebrovascular density remains to be determined. Since VEGF is the key regulator for vasculogenesis and angiogenesis in the organs and tissues including the brain (Rosenstein et al., 1998), and VEGF-A is the most important subtype in the VEGF family for angiogenesis (Ferrara et al., 2003), we examined the expression of VEGF and VEGF-A in the brain by Western Blotting 24 h after the final treatment (Fig. 1). Brain tissue was dissected from the left hemisphere and lysed for Western Blot (Fig. 2A). We found that the levels of VEGF ($p < .01$, Fig. 2B and C) and VEGF-A ($p < .05$, Fig. 2D and E) were significantly decreased in the brains of TgNotch3R90C mice as compared to the age-matched WT controls. SCF + G-CSF treatment significantly increased the levels of VEGF and VEGF-A in the brains of TgNotch3R90C mice ($p < .05$, Fig. 2B–E). These data reveal that low levels of VEGF and VEGF-A happen in the brains of TgNotch3R90C mice and that SCF + G-CSF treatment enhances the cerebral production of VEGF and VEGF-A in the CADASIL condition. These findings also suggest that the low levels of VEGF/VEGF-A may play a role in CADASIL pathogenesis, and that increase of VEGF/VEGF-A could be a key mechanistic process for SCF + G-CSF-enhanced angiogenesis and brain repair in the CADASIL condition.

Through immunofluorescence double staining, we also identified the cellular source of VEGF and VEGF-A expression in the brains of TgNotch3R90C mice (Supplementary Fig. 1). Using the signature markers for neurons (neuronal nuclei, NeuN), astrocytes (glial fibrillary acidic protein, GFAP), microglial cells (ionized calcium binding adaptor molecule 1, Iba1), oligodendrocytes (2′,3′-Cyclic-nucleotide 3′-phosphodiesterase, CNPase), VSMCs (alpha-smooth muscle actin, α-SMA), and ECs (CD31), we observed that both the VEGF and VEGF-A were expressed in cerebral neurons, astrocytes, microglial cells, VSMCs, and ECs, while oligodendrocytes did not show immunopositive to VEGF and VEGF-A. These findings are in line with previous studies (Smith et al., 2001; Cao et al., 2004; Ryu et al., 2009; Talwar and Srivastava, 2014). We also noted that both VEGF and VEGF-A are abundantly expressed in the cells of cerebrovascular wall (VSMCs and ECs) (Supplementary Fig. 1).

3.2. SCF + G-CSF-improved spatial learning and memory are prevented by Avastin in TgNotch3R90C mice

Our previous study has revealed that SCF + G-CSF not only increases cerebrovascular density but it also improves spatial learning and memory as shown by water maze testing in TgNotch3R90C mice (Liu et al., 2015). To elucidate the causal relationship between the improved cognitive function and restored cerebral blood vessel densities by SCF + G-CSF treatment in TgNotch3R90C mice, we utilized Avastin to block SCF + G-CSF-enhanced angiogenesis and evaluated the spatial learning and memory by water maze testing. Avastin, a humanized monoclonal antibody that neutralizes VEGF-A, has been proven to prevent new blood vessel generation in cancer and the disease with pathological angiogenesis (Flieger et al., 2006; Andreoli and Miller, 2007; Mitchell et al., 2008). Avastin has shown effectiveness in blocking VEGF and angiogenesis in mice (Feng et al., 2014; Jiang et al., 2014).

The water maze test was performed 7 weeks after the final treatment of Avastin and SCF + G-CSF given at 10 months of age. During the five-day testing, we observed that TgNotch3R90C mice with different treatments showed different patterns of spatial learning and memory. On the first day of the testing, all the TgNotch3R90C mice showed increased latencies finding the hidden platform (increased escape latencies) as compared to the WT mice ($p < .05$, Fig. 3), suggesting the impairments of spatial cognition in TgNotch3R90C mice. On day 2 and day 3, TgNotch3R90C mice with vehicle injection showed significantly longer escape latency than those in the WT group (day 2 $p < .01$, day 3 $p < .01$, Fig. 3). These findings further confirmed the deficits of TgNotch3R90C mice in spatial learning and memory. By contrast, the escape latency of SCF + G-CSF-treated TgNotch3R90C mice displayed a continuous decrease during the day 2 and day 3 testing, and this reduction reached a significant level in day 3 testing as compared to the TgNotch3R90C vehicle control mice ($p < .05$, Fig. 3). These findings were consistent with our previous data showing improved spatial learning and memory in TgNotch3R90C mice by SCF + G-CSF treatment (Liu et al., 2015). In addition, we also observed that the escape latency of the TgNotch3R90C mice treated with both Avastin and SCF + G-CSF was significantly prolonged when compared to the SCF + G-CSF-treated TgNotch3R90C mice in day 3 testing ($p < .05$, Fig. 3), suggesting that the SCF + G-CSF-improved spatial learning and memory was eliminated by Avastin. This observation also suggests that SCF + G-CSF-enhanced cerebrovascular regeneration might be crucially involved in cognitive recovery in the CADASIL mouse model (TgNotch3R90C).

3.3. Avastin blocks SCF + G-CSF-increased vascular density in the brains of TgNotch3R90C mice

We then sought to determine whether Avastin eliminates SCF + G-CSF-enhanced vascular generation. To this end, we measured the

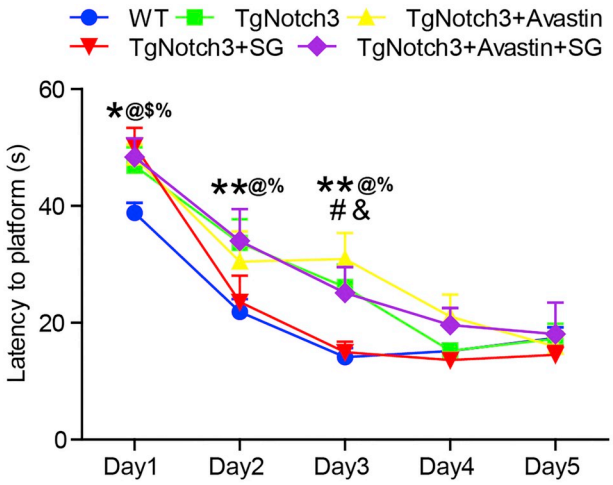

Fig. 3. SCF + G-CSF treatment-improved spatial learning and memory in TgNotch3R90C mice are prevented by Avastin pretreatment. The spatial learning and memory were examined using a water maze test. Data were collected from four independent trails per day for five consecutive days. Mean ± S.E.M. $N = 8–14$. *p < .05, **p < .01; TgNotch3R90C vehicle control mice *vs.* WT mice. @ p < .05, TgNotch3R90C + Avastin group *vs.* WT group. $p < .05, TgNotch3R90C + SG group *vs.* WT group. % p < .05, TgNotch3R90C + Avastin + SG group *vs.* WT group. #p < .05, TgNotch3R90C + SG mice *vs.* TgNotch3R90C vehicle control mice. &p < .05, TgNotch3R90C + Avastin + SG group *vs.* TgNotch3R90C + SG group. Two-way repeated ANOVA with Tukey *post hoc* test. WT: wild type. TgNotch3: TgNotch3R90C. SG: SCF + G-CSF.

cerebral blood vessel density in the cortex, striatum and hippocampus through lectin staining (Fig. 4A–T). We observed that lectin positive cerebral blood vessels were significantly reduced in the cortex, striatum and hippocampus in the TgNotch3R90C control mice as compared to the WT mice (cortex and hippocampus: Tg-vehicle controls and Tg-Avastin controls *vs.* WT controls, p < .001; striatum: Tg-vehicle controls *vs.* WT controls, p < .05, Tg-Avastin controls *vs.* WT controls, p < .01; Fig. 4C–T), suggesting vasculature loss in the brains of TgNotch3R90C mice. The Notch3R90C mutation-induced vasculature loss was completely restored in the cortex and striatum by SCF + G-CSF treatment (Tg-S + G *vs.* Tg-vehicle controls, p < .01; Tg-S + G *vs.* WT controls, no difference; Fig. 4C–L, R and S), and the vascular density was significantly increased in the hippocampus of SCF + G-CSF-treated TgNotch3R90C mice as compared to the TgNotch3R90C vehicle controls (p < .05, Fig. 4M–Q and T). To determine whether the SCF + G-CSF-increased cerebrovascular density is mediated by the enhancement of angiogenesis, 2-day-BrdU injections were performed during SCF + G-CSF treatment (Fig. 5A). We observed that $BrdU^+CD31^+$ endothelial cells in the cerebrovascular walls were significantly increased after 5-day-SCF + G-CSF treatment in TgNotch3R90C mice as compared to the vehicle controls (Fig. 5B and C). These observations indicate that SCF + G-CSF treatment enhances cerebrovascular regeneration (angiogenesis) and restores vasculature in the brains of TgNotch3R90C mice. Injecting Avastin before administering SCF + G-CSF completely blocked the SCF + G-CSF-increased vascular densities in the cortex, striatum and hippocampus of the TgNotch3R90C mice (p < .01, Fig. 4R–T), while the blood vessel density in the three brain regions did not show differences between the TgNotch3R90C vehicle controls and TgNotch3R90C Avastin controls (p > .05. Fig. 4 R-T). These findings suggest that VEGF-A is required for SCF + G-CSF-enhanced cerebrovascular regeneration in TgNotch3R90C mice. The Avastin dose used in this study does not negatively affect cerebral vasculature in adult TgNotch3R90C mice, in which the levels of VEGF-A and vessel density are lower than WT mice.

3.4. Avastin eliminates SCF + G-CSF-increased EC proliferation and angiogenesis

To further confirm the *in vivo* data that SCF + G-CSF treatment increases cerebrovascular regeneration in TgNotch3R90C mice through VEGF-A, we performed an *in vitro* study by using primary cultured ECs isolated from the brains of TgNotch3R90C mice and WT mice.

Purification of ECs was analyzed before initiating the experiments. As shown in Fig. 6A–D, > 92% passage 1 ECs isolated from the brains of WT and TgNotch3R90C mice were CD31 positive ECs.

In cell proliferation assay, we observed that BrdU positive ECs were significantly decreased in the TgNotch3R90C group as compared to the WT controls (p < .05), while SCF + G-CSF treatment completely restored the $BrdU^+$ cells in TgNotch3R90C group (p < .01) (Fig. 6E–H). Similar results were also found by Ki-67 immunostaining (Fig. 6I–L). These data indicate that Notch3R90C mutation-decreased cerebral EC proliferation is restored by SCF + G-CSF treatment. We then sought to determine whether SCF + G-CSF enhances EC proliferation through VEGF-A. To this end, VEGF-A inhibitor, Avastin, was added to the ECs before SCF + G-CSF treatment. We found that the SCF + G-CSF-enhanced EC proliferation (increased $BrdU^+$ and Ki-67^+ ECs) was completely eliminated by Avastin (p < .01) (Fig. 6M–V).

We also determined angiogenesis through tube formation assay. Our data revealed that both the number and total length of branches in TgNotch3R90C-ECs were significantly decreased in comparison with the WT-ECs (p < .01), while SCF + G-CSF-treated TgNotch3R90C-ECs showed significant increases in both the number and total length of branches (p < .05) (Fig. 6W-A′). In addition, the SCF + G-CSF-increased the number and total length of branches in TgNotch3R90C-ECs were totally blocked by Avastin pretreatment (p < .01) (Fig. 6B′–G′).

Altogether, these findings validate our *in vivo* data and confirm that Notch3R90C mutation causes reduced angiogenesis and that SCF + G-CSF treatment enhances angiogenesis in TgNotch3R90C mice through VEGF-A.

3.5. Avastin blocks SCF + G-CSF-increased neuron structure densities in both the cortex and hippocampus of TgNotch3R90C mice

Neural structure changes play an important role in brain functioning in both physical and pathological conditions (Holtmaat et al., 2006; Brown et al., 2007; Xu et al., 2009; Yang et al., 2009; Cui et al., 2015; Cui et al., 2016). Consequently, we sought to determine whether SCF + G-CSF-enhanced cerebral angiogenesis is involved in remodeling of neural structures in TgNotch3R90C mice.

To determine whether SCF + G-CSF treatment promotes neuron structure regeneration in the brains of TgNotch3R90C mice, we examined dendritic and axonal densities in the cortex and hippocampus through MAP2 and SMI312 immunohistochemistry. MAP2 is one of the most prominent proteins concentrated in the dendrites of neurons and regulates dendritic growth (Johnson and Jope, 1992; Dehmelt and Halpain, 2005). SMI312 is a pan marker of neurofilaments providing structural support for axons and regulates axonal structure changes (Ulfig et al., 1998). The densities for $MAP2^+$ dendrites and $SMI312^+$ axons in cortical layer 1, and 4–6 did not show significant differences among the experimental groups (data not shown); however, as shown in Fig. 7 (A-T), MAP2 positive dendrites and SMI312 positive axons in both the cortical layer 2/3 and hippocampal CA1 region were significantly reduced in the TgNotch3R90C control mice when compared to the WT mice (cortex: MAP2, p < .05; SMI312, p < .01; hippocampus: MAP2, p < .01; SMI312, p < .05; Fig. 7), suggesting reduced neural structures in these brain regions of TgNotch3R90C mice. There were no differences between the two TgNotch3R90C control groups (vehicle and Avastin controls) in the densities of $MAP2^+$ dendrites and $SMI312^+$ axons in the cortical layer 2/3 and hippocampal CA1 region

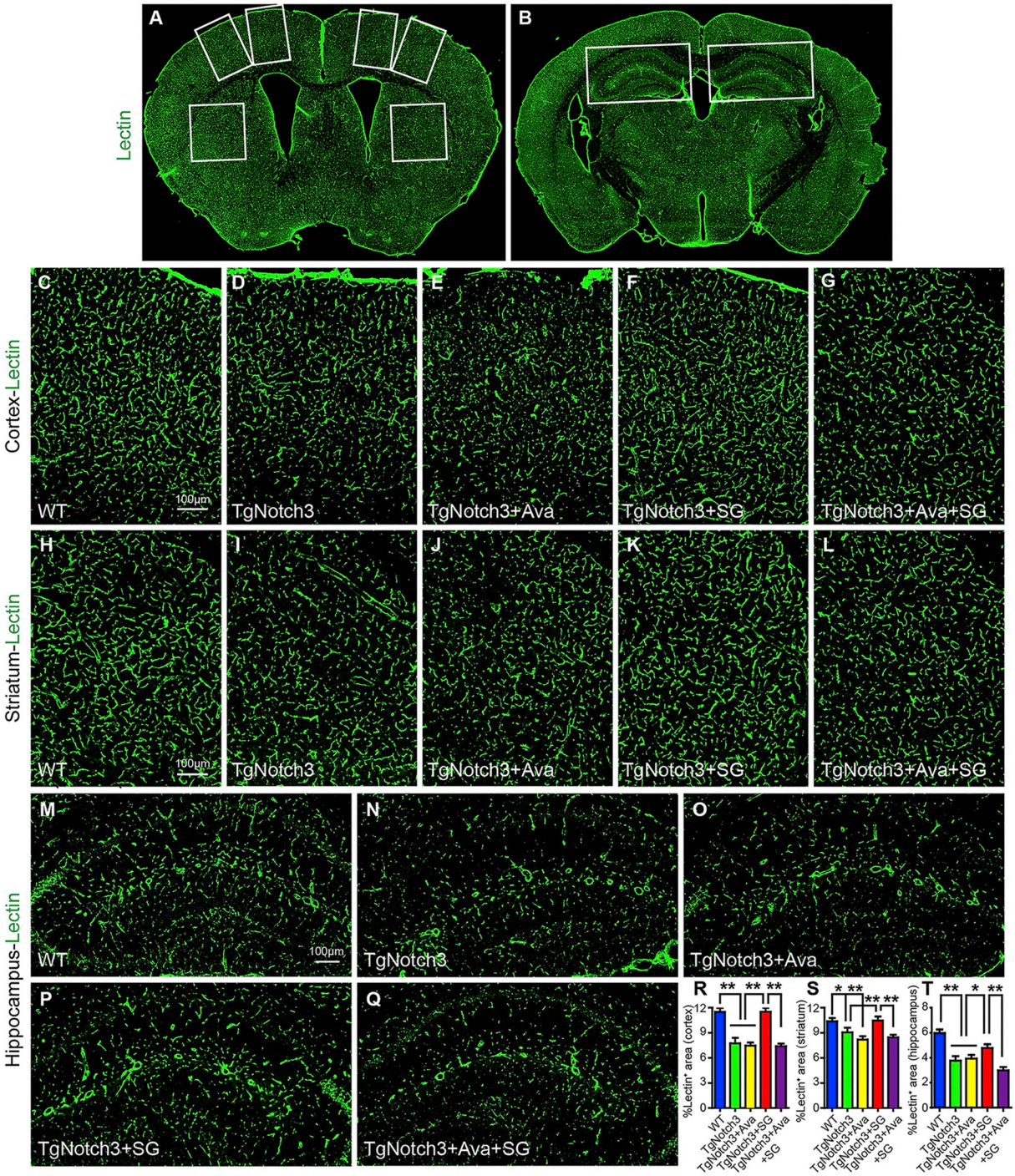

Fig. 4. Cerebral vessel density assessment data. Note that reduced cerebral vessel densities in the cortex, striatum, and hippocampus of TgNotch3R90C mice are restored by SCF + GCSF treatment. The SCF + G-CSF-enhanced angiogenesis is completely eliminated by Avastin pretreatment. Cerebral vessel densities were identified by lectin staining. (A-B) Schematic diagrams indicate the imaging areas in the cortex, striatum and hippocampus. (C-Q) Representative images of lectin positive vessels in the cortex (C-G), striatum (H-L), and hippocampus (M-Q). (R-T) Statistical data of lectin positive areas in the cortex (R), striatum (S) and hippocampus (T). Mean ± S.E.M. $N = 7–11$. *$p < .05$, **$p < .01$. One-way ANOVA with Tukey *post hoc* test. Scale bars: C-Q, 100 μm. WT: wild type. TgNotch3: TgNotch3R90C. SG: SCF + G-CSF. Ava: Avastin. (For interpretation of the references to colour in this figure legend, the reader is referred to the web version of this article.)

(Fig. 7). SCF + G-CSF treatment, however, showed significant increases in $MAP2^+$ dendrites and $SMI312^+$ axons in both the cortical layer 2/3 and hippocampal CA1 as compared to the vehicle control TgNotch3R90C mice (cortex: MAP2, $p < .01$; SMI312, $p < .05$; hippocampus: MAP2, $p < .01$; SMI312, $p < .01$; Fig. 7), while the SCF + G-CSF-increased dendrites and axons were not different from the WT controls. These data indicate that the impaired neural structures in the brains of TgNotch3R90C mice are repaired by SCF + G-CSF treatment.

We also found that the SCF + G-CSF-increased dendrites and axons in the cortical layer 2/3 and hippocampal CA1 region of TgNotch3R90C mice were entirely eliminated by the Avastin pretreatment (cortex: MAP2, $p < .05$; SMI312, $p < .01$; hippocampus: MAP2, $p < .01$; SMI312, $p < .01$; Fig. 7), suggesting that VEGF-A-mediated angiogenic process may be involved in the SCF + G-CSF-enhanced dendritic and

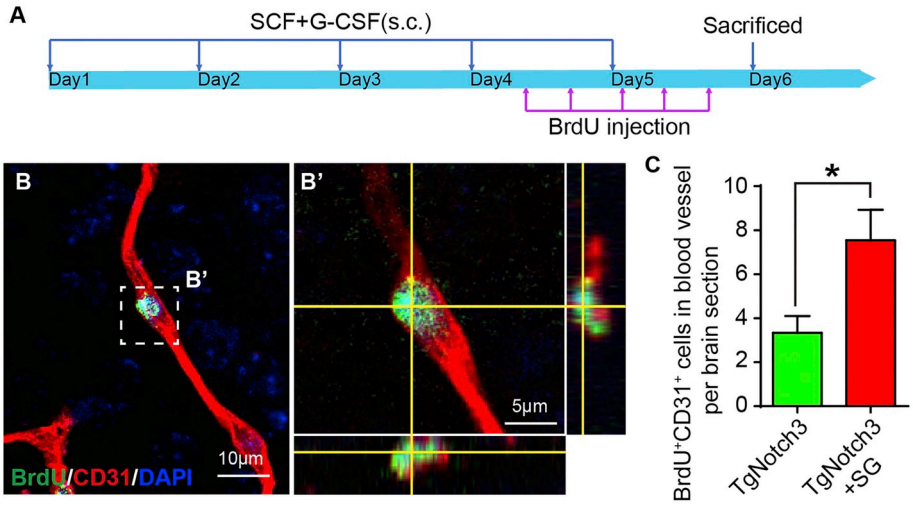

Fig. 5. Cerebral endothelial cell proliferation is enhanced by SCF + G-CSF treatment in TgNotch3R90C mice. (A) Schematic flowchart of the experiment. SCF + G-CSF was subcutaneously (s.c.) injected to TgNotch3R90C mice for five consecutive days. An equal volume of vehicle solution was injected in the control TgNotch3R90C mice. BrdU was intraperitoneally injected for the last two days of SCF + G-CSF treatment. Mice were euthanized within 24 h after the final injection of BrdU for immunohistochemistry analysis. (B and B′) Representative confocal images show immunofluorescence double labeling of a BrdU$^+$ and CD31$^+$ (BrdU-green, CD31-red) cell in the capillary wall. (C) Statistical data reveal that the number of BrdU$^+$ CD31$^+$ cells in the brains of TgNotch3R90C mice is significantly increased by SCF + G-CSF. Mean ± S.E.M. N = 3. *p < .05. Unpaired *t*-test. TgNotch3: TgNotch3R90C. SG: SCF + G-CSF. (For interpretation of the references to colour in this figure legend, the reader is referred to the web version of this article.)

axonal regeneration in the brains of TgNotch3R90C mice.

To confirm the relationship between the SCF + G-CSF-enhanced dendritic and axonal regeneration and angiogenesis in the cortical layer 2/3 and hippocampal CA1 of TgNotch3R90C mice, we specifically quantified cerebral vascular densities in the cortical layer 2/3 and hippocampal CA1 (Fig. 8A-P). In line with our observations in the entire cortex, striatum and hippocampus, our findings revealed that lectin$^+$ blood vessels in the cortical layer 2/3 were significantly decreased in TgNotch3R90C vehicle controls as compared to the WT controls (% lectin$^+$ area: $p < .01$; length of lectin$^+$ vessels: $p < .05$; Fig. 8A, B, K and M). SCF + G-CSF treatment significantly increased blood vessels in the cortical layer 2/3 of TgNotch3R90C mice as compared to the TgNotch3R90C vehicle controls (% lectin$^+$ area: $p < .01$; length of lectin$^+$ vessels: $p < .05$; Fig. 8B,D, K and M), and the blood vessel density of SCF + G-CSF-treated TgNotch3R90C mice was not different from the WT controls ($p > .05$, Fig. 8A, D, K and M), suggesting that the impaired blood vessels in the cortical layer 2/3 of TgNotch3R90C mice are restored by the SCF + G-CSF treatment. Avastin pretreatment completely eliminated the SCF + G-CSF-increased lectin$^+$ cerebral blood vessels in the cortical layer 2/3 ($p < .01$, Fig. 8D, E, K and M).

In addition to the cortex, we also found similar results in the hippocampal CA1 region. The reduced lectin$^+$ blood vessels in the TgNotch3R90C vehicle control mice (% lectin$^+$ area: $p < .01$; length of lectin$^+$ vessels: $p < .05$) were restored by the SCF + G-CSF treatment ($p < .05$, Fig. 8F-I, L and N), while the SCF + G-CSF-increased blood vessel density was totally removed by Avastin pretreatment ($p < .01$, Fig. 8F-J, L and N). No differences were found in the cerebral blood vessel densities between the TgNotch3R90C vehicle controls and TgNotch3R90C Avastin controls (Fig. 8).

The alterations of cerebral blood vessel densities in both the cortical layer 2/3 and hippocampal CA1 region of TgNotch3R90C mice were further validated by immunohistochemistry using an EC marker, CD31. The findings of CD31$^+$ blood vessels were consistent with the data of lectin$^+$ blood vessels (Supplementary Fig. 2).

To further elucidate the relationship between angiogenesis and regeneration of dendrites and axons, a correlation test was performed. Our data revealed that the blood vessel densities in the cortical layer 2/3 and hippocampal CA1 regions were significantly and positively correlated to the densities of dendrites and axons in the same regions of the experimental mice ($p < .001$, Fig. 7O–R). These findings suggest a positive dependence between SCF + G-CSF-enhanced angiogenesis and neurostructural regeneration.

3.6. SCF + G-CSF-increased synaptogenesis is blocked by Avastin in TgNotch3R90C mice

Synaptic degeneration is a key pathology of cognitive impairments (Robinson et al., 2014; Bereczki et al., 2018). In addition to the dendritic and axonal changes, we wanted to know whether synaptic alterations also occur in the brains of TgNotch3R90C mice treated with or without SCF + G-CSF.

Synaptophysin is a glycoprotein found in the presynaptic vesicles (Wiedenmann et al., 1986), and PSD-95 is a membrane-associated scaffolding protein that exclusively appears in the post-synaptic density (PSD) of neurons (Hunt et al., 1996). Using synaptophysin and PSD-95 as the markers for presynapses and postsynapses, respectively, we quantified the synaptic densities through immunohistochemistry. As presented in Fig. 9 (A-P), in both the cortical layer 2/3 and hippocampal CA1 region, synaptophysin$^+$ presynapses were significantly reduced in TgNotch3R90C control mice (vehicle and Avastin controls) as compared to WT mice ($p < .01$). No differences were found in the reduced synaptophysin$^+$ presynapses between the two TgNotch3R90C control groups (vehicle and Avastin controls) (Fig. 9). SCF + G-CSF-treated TgNotch3R90C mice, however, showed significant increases in synaptophysin$^+$ presynapses in both the cortical layer 2/3 ($p < .01$, Tg-S + G *vs.* Tg-vehicle controls; Fig. 9B, D &K) and hippocampal CA1 region ($p < .05$, Tg-S + G *vs.* Tg- vehicle controls; Fig. 9G, I &L), while the SCF + G-CSF-increased synaptophysin$^+$ presynapses were not different from the WT controls (Fig. 9K&L). The SCF + G-CSF-increased presynapses in the cortex and hippocampus were completely blocked by Avastin pretreatment ($p < .01$, Fig. 9K&L). Moreover, correlation analysis data showed a significantly positive correlation between blood vessel density and presynaptic density in both the cortical layer 2/3 and hippocampal CA1 region ($p < .001$, Fig. 9M and N). Similar findings were observed in PSD-95-labled postsynapses. In cortical layer 2/3, TgNotch3R90C control mice (vehicle controls and Avastin controls) displayed significant reductions in PSD-95$^+$ postsynapses as compared to WT controls (% of PSD-95$^+$ area: $p < .01$; PSD-95$^+$ puncta: $p < .05$, Supplementary Fig. 3). There were no differences between the TgNotch3R90C vehicle and Avastin controls. The PSD-95$^+$ postsynapses in the cortical layer 2/3 of SCF + G-CSF-treated TgNotch3R90C mice were significantly increased when compared to vehicle control TgNotch3R90C mice ($p < .01$, Supplementary Fig. 3). The levels of SCF + G-CSF-increased PSD-95$^+$ postsynapses were not different from the WT controls, while the SCF + G-CSF-increased PSD-95$^+$ postsynapses in the cortical layer 2/3 were totally removed by

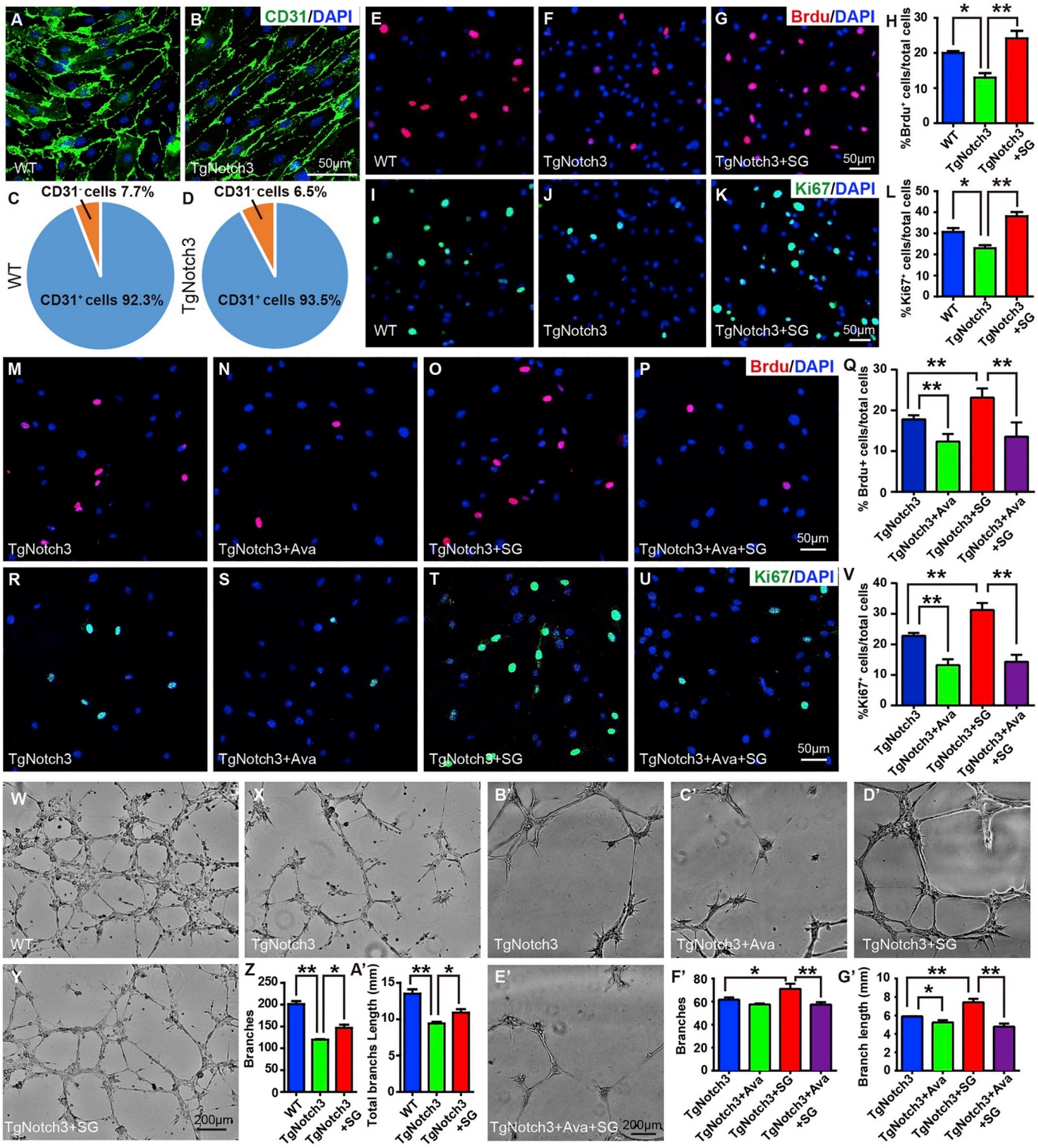

Fig. 6. Cerebral endothelial cell proliferation and tube formation. Note that reduced endothelial cell (EC) proliferation and tube formation in the TgNotch3R90C mouse brain-isolated ECs are restored by SCF + G-CSF treatment. Avastin pretreatment eliminates the SCF + G-CSF-increased EC proliferation and tube formation. (A-D) Purification of primary cultured CD31$^+$ ECs (passage 1). DAPI: nuclear counterstain. (*E*-V) EC proliferation data. EC proliferation were identified by BrdU (red) and Ki67 (green) immunocytochemistry. (W-G′) Tube formation data. (W-Y, B′-E′) Representative images of tube formation. (Z, A′, F′ and G′) Statistical data of the number of branches and the total branch length in the primary cultured ECs. Mean ± S.E.M. Experiments were independently repeated 3 times. *p < .05, **p < .01. One-way ANOVA with Tukey *post hoc* test. Scale bars: A-U, 50 μm. W-E′, 200 μm. WT: wild type. TgNotch3: TgNotch3R90C. SG: SCF + G-CSF. Ava: Avastin. (For interpretation of the references to colour in this figure legend, the reader is referred to the web version of this article.)

Avastin pretreatment (p < .01, Supplementary Fig. 3). The correlation of PSD-95$^+$ postsynapses in the cortical layer 2/3 was significantly positive to the blood vessel density in the same brain regions (p < .001, Supplementary Fig. 3). The data of PSD-95$^+$ postsynapses in the hippocampus, however, did not show significant differences among the experimental groups (data not shown).

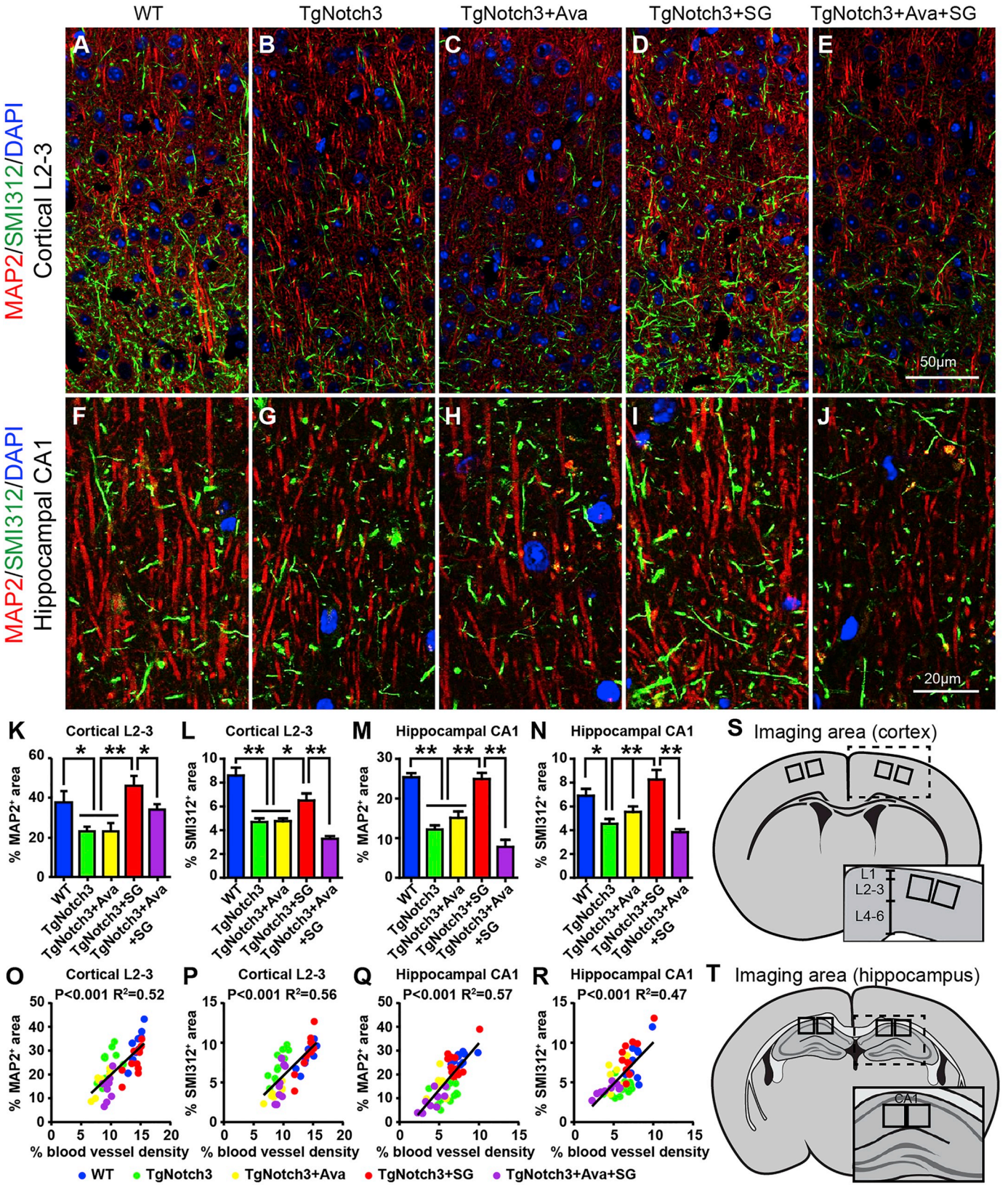

(caption on next page)

Fig. 7. Dendritic and axonal density assessment data. Note that reduced neural network densities in both the cortical layer 2/3 and hippocampal CA1 of TgNotch3R90C mice are restored by SCF + G-CSF treatment. Avastin pretreatment completely eliminates the SCF + G-CSF-increased neural network regeneration in the cortical layer 2/3 and hippocampal CA1 of TgNotch3R90C mice. The neural network densities are positively correlated to the cerebrovascular densities in the cortical layer 2/3 and hippocampal CA1. Neural structural networks were identified by MAP2 (dendrite, red) and SMI312 (axon, green) immunostaining. (A-J) Representative images of double immunofluorescence staining for MAP2 and SMI312 in the cortical layer 2/3 region (A-E) and hippocampal CA1 region (F-J). (K-N) Statistical data of MAP2 and SMI312 positive area in the cortical layer 2/3 (K and L) and hippocampal CA1 regions (M and N). (O-R) Positive correlation between the vessel densities and neural network densities in the cortical layer 2/3 (O and P) and hippocampal CA1 region (Q and R). (S and T) Schematic diagrams indicate the imaging areas in the cortex and hippocampus. Mean ± S.E.M. N = 7–11. *p < .05, **p < .01. One-way ANOVA with Tukey *post hoc* test. Scale bars: A-E, 50 μm; F-J, 20 μm. DAPI: nuclear counterstaining. WT: wild type. TgNotch3: TgNotch3R90C. SG: SCF + G-CSF. Ava: Avastin. (For interpretation of the references to colour in this figure legend, the reader is referred to the web version of this article.)

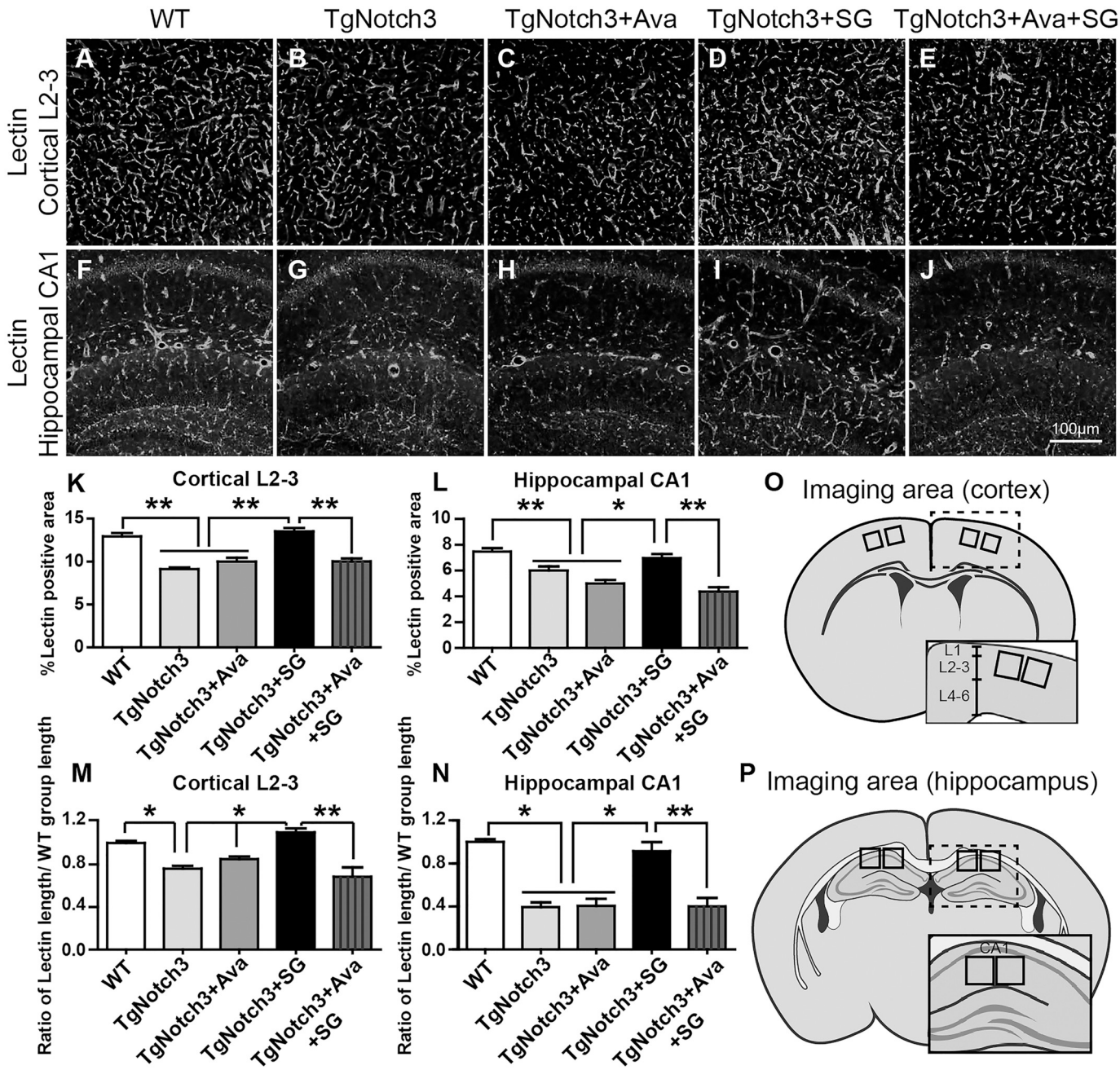

Fig. 8. Regional blood vessel density examination data. Note that reduced vessel densities in both the cortical layer 2/3 and hippocampal CA1 region of TgNotch3R90C mice are restored by SCF + G-CSF treatment, while the SCF + G-CSF-enhanced angiogenesis is completely eliminated by Avastin pretreatment. Cerebral vessel densities were identified by lectin staining. (A-E) Representative images of lectin positive vessels in the cortical layer 2/3 region. (F-J) Representative images of lectin positive vessels in the hippocampal CA1 region. (K and L) Statistical data of lectin positive area in the cortical layer 2/3 and hippocampal CA1 regions. (M and N) Statistical data of lectin positive vessel length in the cortical layer 2/3 and hippocampal CA1 regions. (O and P) Schematic diagrams show the imaging areas in the cortex and hippocampus. Mean ± S.E.M. N = 7–11. *p < .05, **p < .01. One-way ANOVA with Tukey *post hoc* test. Scale bar, 100 μm for A-J. WT: wild type. TgNotch3: TgNotch3R90C. SG: SCF + G-CSF. Ava: Avastin. (For interpretation of the references to colour in this figure legend, the reader is referred to the web version of this article.)

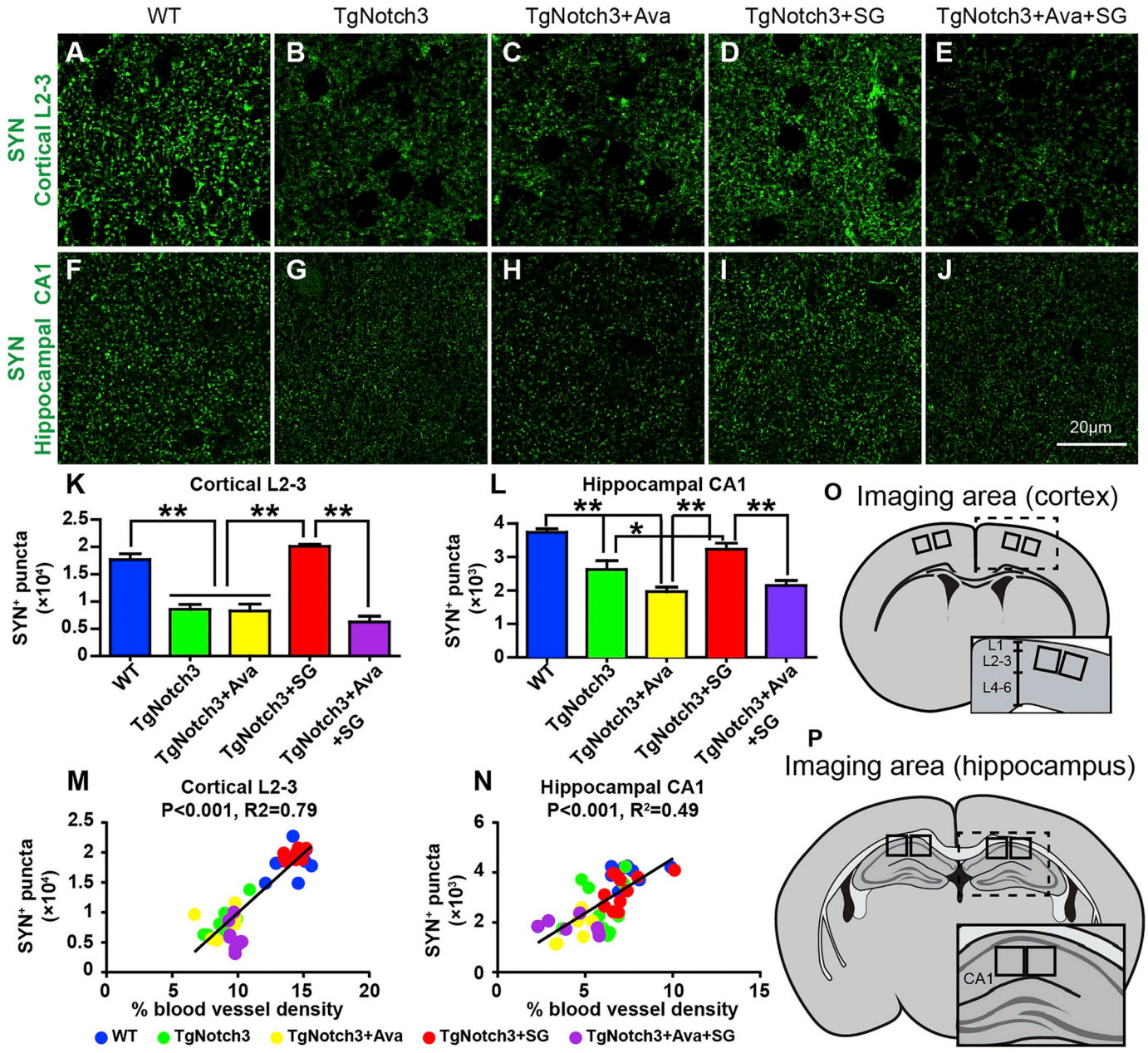

Fig. 9. Synaptic analysis data. Note that reduced synapses in both the cortical layer 2/3 and hippocampal CA1 region of TgNotch3R90C mice are restored by SCF + G-CSF treatment. Avastin pretreatment totally blocks the SCF + G-CSF-increased synaptogenesis in the cortical layer 2/3 and hippocampal CA1 regions of TgNotch3R90C mice. The synaptic densities are positively correlated to the cerebrovascular densities in the cortical layer 2/3 and hippocampal CA1 regions. The synaptic density was examined through synaptophysin immunostaining (green). (A-J) Representative images of synaptophysin positive presynapses in the cortical layer 2/3 (A-E) and hippocampal CA1 region (F-J). (K and L) Statistical data of the number of synaptophysin positive puncta in the cortical layer 2/3 (K) and hippocampal CA1 region (L). (M and N) Positive correlation between the number of synaptophysin positive puncta and cerebral vessel densities in the cortical layer 2/3 and hippocampal CA1 regions. (O and P) Schematic diagrams reveal the imaging areas in the cortex and hippocampus. Mean ± S.E.M. N = 7–11. *p < .05, ** p < .01. One-way ANOVA with Tukey *post hoc* test. Scale bar, 20 μm for A-J. WT: wild type. TgNotch3: TgNotch3R90C. SG: SCF + G-CSF. Ava: Avastin. (For interpretation of the references to colour in this figure legend, the reader is referred to the web version of this article.)

Taken altogether, these findings suggest that synaptic degeneration occurs in the cortical layer 2/3 and hippocampal CA1 regions of TgNotch3R90C mice. SCF + G-CSF treatment prevents the synaptic degeneration through the VEGF-A-mediated angiogenesis.

3.7. SCF + G-CSF-enhanced neurogenesis is eliminated by Avastin in TgNotch3R90C mice

It has been shown that there is a coupling relationship between neurogenesis and angiogenesis in the developing brain (Madelaine et al., 2017) and in adult brain after ischemic stroke (Ruan et al., 2015). Based on our findings of cerebral vessel densities, we hypothesized that reduced cerebral vessel densities in TgNotch3R90C mice might also lead to decreased neurogenesis. To test this hypothesis, we quantified neuronal precursor cells and immature neurons in both the subventricular zone (SVZ) and subgranular zone (SGZ) through DCX immunostaining. DCX, a microtubule-associated protein, is specifically expressed in the neuronal precursor cells and immature neurons during the period of neurogenesis in both developing and adult central nervous system (Gleeson et al., 1999; Brown et al., 2003). The data shown in

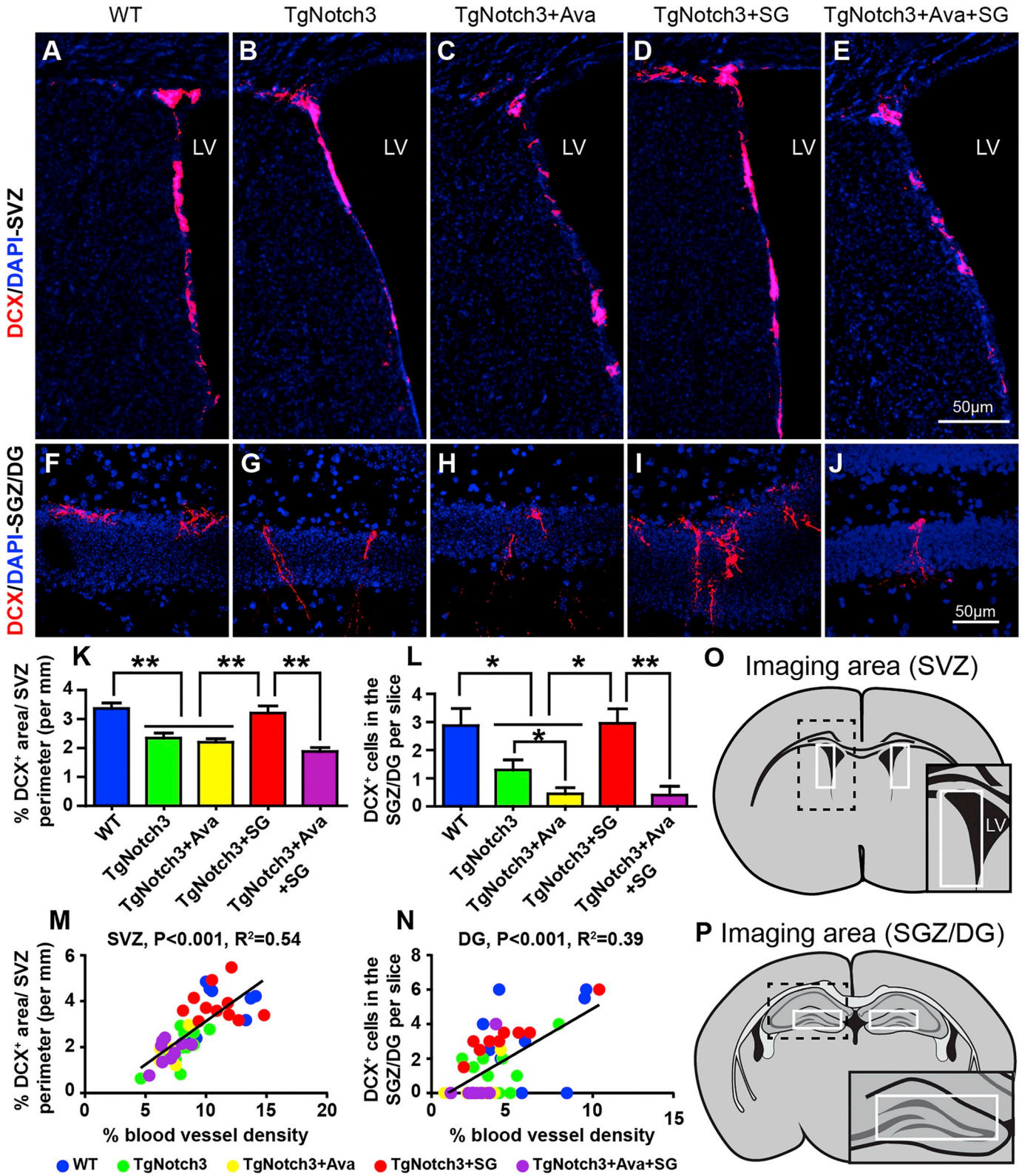

Fig. 10. Neurogenesis assessment data. Note that reduced neurogenesis in both the subventricular zone (SVZ) and subgranular zone (SGZ) of TgNotch3R90C mice are restored by SCF + G-CSF treatment. Avastin pretreatment completely eliminates the SCF + G-CSF-enhanced neurogenesis. The neurogenic densities are positively correlated to the vascular densities in the regions of SVZ and dentate gyrus (DG). Neurogenesis was identified by doublecortin (DCX) immunostaining. (A-J) Representative images of DCX positive cells in the SVZ (A-E) and SGZ/DG (F-J). (K) Statistical data of DCX positive area in the SVZ. The DCX positive area in the SVZ was corrected by the length of the SVZ. One-way ANOVA with Tukey *post hoc* test. (L) Statistical data of the number of DCX positive cells in the SGZ/DG. Kruskal-Wallis test with Dunn's multiple comparison test. (M and N) Positive correlation between neurogenic densities and blood vessel densities in the SVZ (M) and the SGZ/DG region (N). (O and P) Schematic diagrams indicate the imaging areas in the SVZ and SGZ/DG. Mean ± S.E.M. N = 7–11. *p < .05, **p < .01. Scale bars, 50 μm for A-J. DAPI: nuclear counterstaining. WT: wild type. TgNotch3: TgNotch3R90C. SG: SCF + G-CSF. Ava: Avastin.

Fig. 10 (A-P) revealed that DCX positive area in the SVZ ($p < .01$) and DCX^+ cells in the SGZ ($p < .05$) were significantly decreased in TgNotch3R90C mice (Tg-vehicle and Tg-Avastin controls *vs.* WT controls), suggesting reduced neurogenesis in the CADASIL condition. TgNotch3R90C Avastin controls showed further reduction of neurogenesis in the SGZ but not in the SVZ as compared to the TgNotch3R90C vehicle controls ($p < .05$). Compared to the TgNotch3R90C vehicle controls, SCF + G-CSF treatment significantly increased DCX^+ cells in both the SVZ ($p < .01$) and SGZ ($p < .05$), which did not differ from the WT controls. The SCF + G-CSF-enhanced neurogenesis in TgNotch3R90C mice was totally eliminated by the Avastin pretreatment ($p < .01$). In addition, the neurogenesis in both the SVZ and SGZ showed significantly positive correlation to the blood vessel densities (vascular density: Supplementary Fig. 4) in the SVZ region and dentate gyrus of experimental mice ($p < .001$, Fig. 10M & N). These observations indicate that SCF + G-CSF treatment restores neurogenesis in the TgNotch3R90C mice through the VEGF-A-mediated angiogenesis.

3.8. SCF + G-CSF-increased neurovascular network regeneration is positively correlated with cognitive improvements in TgNotch3R90C mice

As presented earlier, our findings have demonstrated that SCF + G-CSF-increased neural structure density, synaptogenesis and neurogenesis are positively correlated to the blood vessel density. To find out the interactive relationship between neurovascular structural alterations and cognitive changes, we applied the correlation tests between neurovascular density and escape latency in water maze test. Since the significant differences among all experimental groups were found only on Day3 testing in water maze (Fig. 3), the data of Day3 testing were selected for the correlation analysis. As shown in Fig. 11, the escape latency in water maze test displayed a significantly negative correlation to the blood vessel density in the cortex ($p < .0001$), striatum ($p = .0002$) and hippocampus ($p < .0001$) (Fig. 11A-C), suggesting that increased cerebrovascular density is positively correlated to the improvements in spatial learning and memory (reduced escape latency). Similarly, we also observed significantly negative correlations between the escape latency and dendritic density ($p < .0001$) (Fig. 11D and E), between the escape latency and axonal density ($p < .0001$) (Fig. 11F and G), and between the escape latency and synaptic density ($p < .0001$) (Fig. 11H and I) in both the cortical layer 2/3 and hippocampal CA1. The correlation analysis data indicate that increased densities of cerebral vessels, neural structures, and synapses contribute to cognitive improvements in TgNotch3R90C mice.

4. Discussion

The vast majority of CADASIL patients carry Notch3 mutations in the epidermal growth factor-like repeat (EGFR) 2–5 of the extracellular domain of Notch3 receptor (Joutel, 2011, 2015; Masek and Andersson, 2017). The TgNotch3R90C mouse model of CADASIL used in the present study represents one of the most common forms of CADASIL because the Notch3 mutation is located at EGFR 2 (Monet-Lepretre et al., 2009). This is a well-characterized CADASIL mouse model carrying CADASIL like pathologies in an age-dependent manner. The earliest pathological changes in VSMC structure and cerebrovascular function appear up to the age of 10 months in TgNotch3R90C mice (Ruchoux et al., 2003). To examine the efficacy of SCF + G-CSF treatment in delaying the pathological progression of CADASIL, the treatment was therefore initiated at 9 months of age and repeated at the age of 10 months. After neurobehavioral testing, neurovascular changes were examined at 15 months of age. Using the TgNotch3R90C mouse model of CADASIL, this study has revealed that (1) the reduced levels of cerebral VEGF/VEGF-A in TgNotch3R90C mice are associated with decreased blood vessel density, reduced neural structure density, reduced synapses, and decreased neurogenesis; (2) SCF + G-CSF treatment restores cerebral vasculature of TgNotch3R90C mice by upregulating VEGF-A production; and (3) SCF + G-CSF treatment improves cognitive function and promotes dendritic/axonal genesis, synaptogenesis, and neurogenesis through the VEGF-A-mediated angiogenesis in TgNotch3R90C mice.

4.1. Reduced cerebral VEGF and blood vessel density are involved in the pathogenesis of CADASIL disease

ECs and pericytes are the key players in new blood vessel formation created from existing vessels (angiogenesis) (Welti et al., 2013; Betz et al., 2016; Eilken et al., 2017). VEGF is the initiator triggering angiogenesis, and the entire process of angiogenesis is orchestrated by molecular signaling between ECs and pericytes (Welti et al., 2013). Pericytes play a key role in promoting EC sprouting, stabilization and maturation of the newly formed vessels, especially in the CNS (Welti et al., 2013; Sweeney et al., 2016; Eilken et al., 2017). In adults, cerebral vasculature is quite stable under physiological conditions to maintain the biological functions, while it turns unstable in pathological conditions (Welti et al., 2013; Betz et al., 2016).

In the condition of CADASIL, blood vessel densities are decreased. In the present study, significantly decreased cerebral vessel density was found in 15-month old TgNotch3R90C mice as compared to age-matched WT, which is in line with our previous findings in 22-month old TgNotch3R90C mice (Liu et al., 2015). In the present study, we have also discovered that the capacity of angiogenesis in TgNotch3R90C mouse brain-isolated ECs is reduced as compared to WT mouse brain-isolated ECs. These data demonstrate that reduced cerebral vessel density in adult TgNotch3R90C mice is a NOTCH3 mutation-driven pathology. In addition to our observations in a mouse model of CADASIL, a clinical study showed that blood vessel density both within and outside white matter hyperintensities was reduced in CADASIL patients as compared to the healthy controls by using high-resolution magnetic resonance imaging (De Guio et al., 2014). The decreased cerebral vessel density in CADASIL could be a key pathological process in disease development as it may contribute to reduction of cerebral blood flow, which has been seen in both the CADASIL patients (Tuominen et al., 2004) and TgNotch3R90C mice (Lacombe et al., 2005). It is worth noting that microvascular density is also diminished in the brains of patients with Alzheimer's disease and Down Syndrome (Drachman et al., 2017). Altogether, these findings imply that reduced cerebral vasculature is tightly linked to vascular dementia.

The mechanism underlying CADASIL-reduced cerebral vasculature remains largely unknown. Genetic fate mapping studies have revealed that pericytes and VSMCs belong to the same cell lineage as both of them derive from common progenitors (Volz et al., 2015; Chen et al., 2016). In addition to VSMCs, degenerative pericytes are also detected in the brains of CADASIL patients (Dziewulska and Lewandowska, 2012) and mouse models of CADASIL (TgNotch3R90C and TgNotch3R169C) (Gu et al., 2012; Ghosh et al., 2015). Moreover, EC damage is also found in CADASIL. Morphological changes and functional impairments of ECs have been observed in both the CADASIL patients (Peters et al., 2008; Campolo et al., 2012; Karlsson et al., 2017) and transgenic mouse models (TgNotch3R90C and TgNotch3R169C) (Ruchoux et al., 2003; Ghosh et al., 2015). EC dysfunction evidenced by EC injury and thrombosis in the cerebral small vessels has been seen in TgNotch3R90C mice at the age of 22 months (Ping et al., 2018). The degenerative VSMCs and pericytes, and EC damage in CADASIL may result in reduction of cerebral vasculature. Importantly, it has been shown that reduced growth factor signaling can lead to vessel retraction and EC apoptosis (Welti et al., 2013; Ambrose, 2017). As stated earlier, VEGF and VEGF-A are vital regulators for angiogenesis (Rosenstein et al., 1998; Ferrara et al., 2003; Welti et al., 2013). The Western Blotting data of the present study have revealed that the levels of VEGF and VEGF-A in the brains of 10–11-month-old TgNotch3R90C mice are significantly decreased as compared to aged-matched WT controls. The

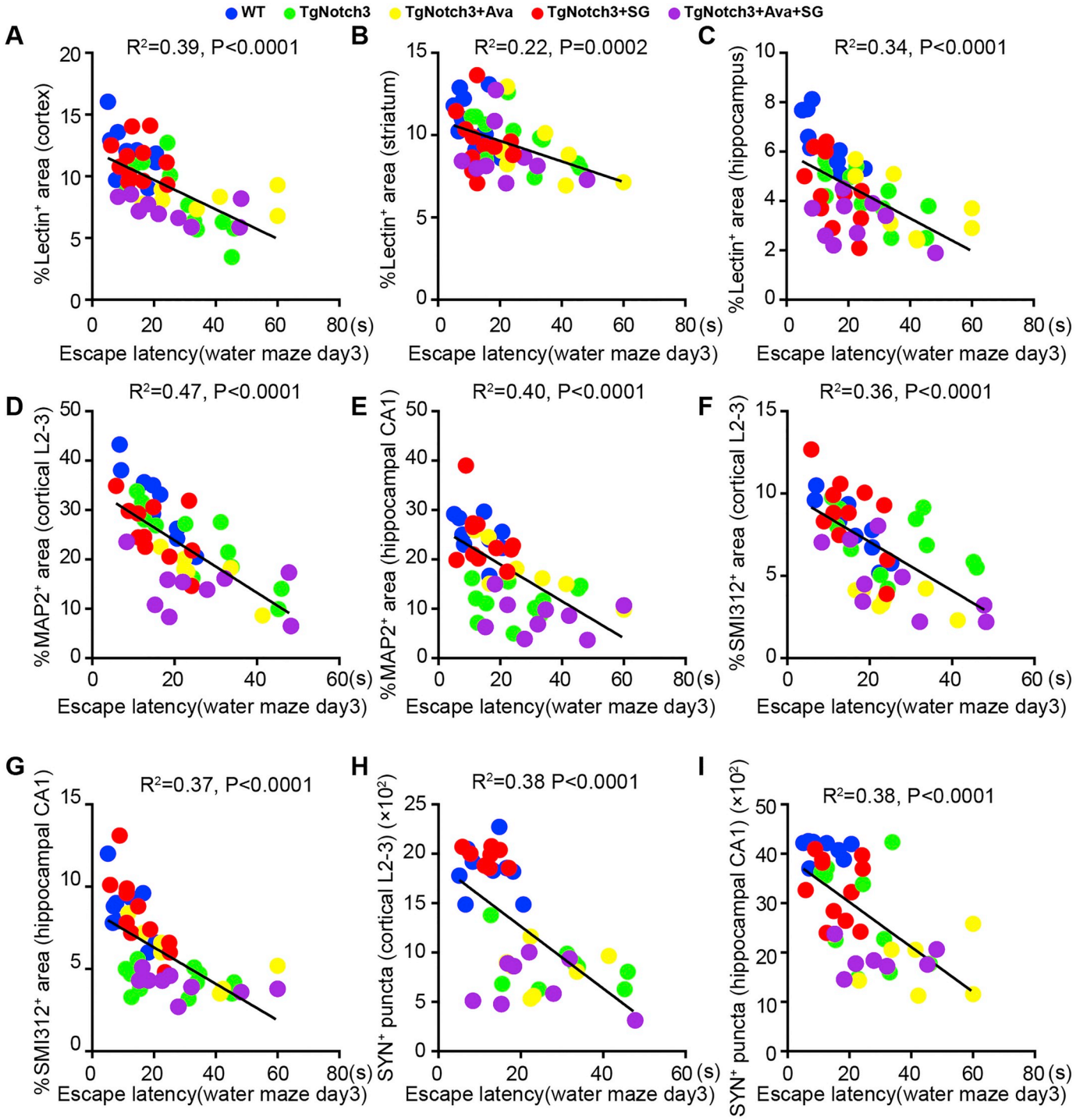

Fig. 11. Correlation analysis data. Note that as the higher densities of cerebral vessels, neural network structures and synapses are identified, the better spatial learning and memory are seen. Increased neurovascular and synaptic densities are significantly correlated with improved spatial learning and memory (reduced escape latency in water maze) in TgNotch3R90C mice. (A–C) Negative correlation is seen between the escape latency (time to find the hidden platform) at day 3 of water maze testing and the cerebral vessel density (lectin$^+$) in the cortex, striatum and hippocampus. (D and E) Negative correlation is shown between the escape latency and dendritic density (MAP2$^+$) in the cortical layer 2/3 and hippocampal CA1. (F and G) Negative correlation is seen between the escape latency and axonal density (SMI312$^+$) in the cortical layer 2/3 and hippocampal CA1. (H and I) Negative correlation is illustrated between the escape latency and synaptic density (SYN$^+$) in the cortical layer 2/3 and hippocampal CA1.

reduced cerebral VEGF and VEGF-A may cause cerebral vessel retraction and vasculature reduction in the TgNotch3R90C mice. However, it remains unclear how the NOTCH3 gene mutation leads to reduced cerebral VEGF and VEGF-A. In addition to VEGF and VEGF-A, Notch signaling in the pericytes (Welti et al., 2013) and VSMCs (Yang et al., 2013) plays a vital role in regulating angiogenesis (Welti et al., 2013), while most CADASIL Notch3 mutations including the R90C mutation do not affect Notch3 signaling (Karlstrom et al., 2002; Joutel et al., 2004; Low et al., 2006; Monet et al., 2007). It would be an open question to be addressed in the future how VEGF and VEGF-A are diminished in CADASIL-associated NOTCH3 mutation.

The findings of the present study have shown that reduced cerebral

vessel density is associated with impaired spatial learning and memory in TgNotch3R90C mice, which is in agreement with our previous observation (Liu et al., 2015). The novel findings of the present study are the demonstrations of decreased dendrites, axons, and synapses in the somatosensory and motor cortex layer 2/3 and in the hippocampal CA1, and reduced neurogenesis in both the SVZ and SGZ in TgNotch3R90C mice. These reductions in neural structures, synapses, and neurogenesis are significantly correlated to decreased cerebral vasculature in the corresponding areas. This positive correlation between decreased cerebral vasculature and reduced neural structures suggests a key role of cerebral vasculature reduction in pathological progression of CADASIL. In reference to our findings, it has been proposed that vessel regression and brain hypoperfusion play an important role in cognitive decline and neurodegeneration in Alzheimer's disease (Zlokovic, 2005). It is relatively easy to understand that the decreased neuron connections in the hippocampal CA1 and reduced neurogenesis in the SGZ lead to impaired spatial learning and memory in TgNotch3R90C mice according to well-accepted body of knowledge (Maguire et al., 2000; Lieberwirth et al., 2016), while an interesting question is how neurovascular reduction in the somatosensory and motor cortex layer 2/3 affects hippocampus-related spatial learning and memory. Recent advances in studying brain function have revealed that the cerebral cortex, a site of neural plasticity and information/memory storage, is crucially involved in higher-order aspects of cognition, memory, and executive function (Badre et al., 2010; Euston et al., 2012; Dum et al., 2016). Somatosensory motor cortex of the human brain contributes to the largest neural networks that organize cognition, emotion and performance (Dum et al., 2016). The excitatory neurons in layer 2/3 of the cortex generate synaptic connections between cortices and hemispheres to integrate information across cortical areas and hemispheres and mediate high-order information processing (Luo et al., 2017; Tjia et al., 2017). Emerging evidence has shown that the layer 2/3 neurons of the somatosensory and motor cortex specifically restore the memory of somatosensory motor experience and learning. Whisker trimming and motor learning promote neural network remodeling and neuronal function modification in the layer 2/3 neurons of the somatosensory and motor cortex in rodents (Kida et al., 2016; Ma et al., 2016). In addition to the cortex, neurogenesis in adult SVZ is necessary for cognitive functions such as perceptual learning and olfactory memory (Valley et al., 2009; Lazarini and Lledo, 2011). Taken all together, these findings suggest that the spatial learning and memory may be generated through a large-scale neural network in the brain including hippocampal CA1 neurons, somatosensory and motor cortex layer 2/3 neurons, and neurogenesis in the SGZ and SVZ. CADASIL Notch3R90C mutation-reduced neurovascular networks in these regions could lead to impairments in the spatial learning and memory.

4.2. SCF + G-CSF treatment enhances brain repair and improves cognitive recovery through VEGF-A-mediated angiogenesis in TgNotch3R90C mice

Our previous study has demonstrated the efficacy of SCF + G-CSF treatment in increasing cerebrovascular density and improving spatial learning and memory in TgNotch3R90C mice (Liu et al., 2015). These findings are further validated in the present study that the Notch3R90C mutation-reduced cerebral vessel density and angiogenesis are restored by SCF + G-CSF treatment, and that the Notch3R90C mutation-impaired spatial learning and memory are improved by the SCF + G-CSF treatment. Moreover, the decreased dendrites, axons, and synapses in both the somatosensory and motor cortex layer 2/3 and hippocampal CA1, and reduced neurogenesis in both the SVZ and SGZ in TgNotch3R90C mice are all restored after SCF + G-CSF treatment. These data reveal that the Notch3R90C mutation-impaired neurovascular networks connecting multiple brain regions that manage spatial learning and memory are repaired by SCF + G-CSF treatment. The SCF + G-CSF-increased cerebral vessels are positively correlated to the SCF + G-CSF-enhanced neural structure regeneration, synaptogenesis, and neurogenesis in TgNotch3R90C mice. Moreover, the increased cerebral vessels, neural structures, and synapses are positively correlated to cognitive improvements in TgNotch3R90C mice. Importantly, once the SCF + G-CSF-enhanced angiogenesis is blocked by Avastin *via* specifically inhibiting VEGF-A, the SCF + G-CSF-improved cognitive function and the SCF + G-CSF-increased neural structure regeneration, synaptogenesis, and neurogenesis in TgNotch3R90C mice are completely eliminated. These new findings suggest that VEGF-A-mediated angiogenesis is required for the SCF + G-CSF-enhanced brain repair and cognitive recovery in the Notch3R90C mutation mouse model of CADASIL.

As stated earlier, our data show that the levels of VEGF and VEGF-A in the brains of TgNotch3R90C mice are reduced, we then asked whether SCF + G-CSF treatment has the ability to promote VEGF and VEGF-A production. Our findings demonstrate that SCF + G-CSF treatment elevates the levels of VEGF and VEGF-A in the brains of TgNotch3R90C mice. The mechanisms as to how SCF + G-CSF enhances cerebral VEGF/VEGF-A production and promotes angiogenesis in Notch3R90C mutant mice remain to be clarified. NF-κB is a transcription factor regulating VEGF expression (Kiriakidis et al., 2003) and angiogenesis (Stoltz et al., 1996). In our previous studies, pretreatment of NF-κB inhibitor leads to elimination of SCF + G-CSF-enhanced angiogenesis, neural structure regeneration, and synaptogenesis in somatosensory motor cortex and removal of the SCF + G-CSF-improved motor function recovery in experimental chronic stroke (Cui et al., 2015; Cui et al., 2016). The involvement of NF-κB in SCF + G-CSF-enhanced cerebral VEGF/VEGF-A production and angiogenesis in the CADASIL condition remains to be further determined in future studies.

Accumulating evidence has revealed the involvement of angiogenesis in drug treatment-induced neurogenesis, synaptogenesis and neurological function improvement in animal models of CNS diseases and injuries. In animal models of ischemic stroke, drug interventions in the acute phase of stroke result in increased angiogenesis and neurogenesis, and improved functional outcome by Metformin treatment (Jin et al., 2014) and promoted angiogenesis and synaptogenesis, and ameliorated neurological deficits by Candesartan treatment (Fouda et al., 2017). Using an APP/PS1 amyloidosis model of Alzheimer's disease, intracerebral delivery of nanospheres encapsulated with VEGF leads to increased angiogenesis, reduced amyloid beta load, and improved cognitive function (Herran et al., 2015). In CNS injury, Premarin treatment enhances angiogenesis and neurogenesis at the lesion site and improves hind limb locomotor function in experimental spinal cord injury (Chen et al., 2010). Atorvastatin treatment increases angiogenesis and synaptogenesis in the boundary region of lesion and CA3 and improves neurological function recovery in experimental brain trauma (Lu et al., 2004). These studies provide additional evidence supporting that angiogenesis plays a vital role in pharmaceutical treatment-enhanced neural repair in the conditions of CNS diseases and injuries.

The limitation of the present study is to reveal novel CADASIL pathology/pathogenesis and mechanisms underlying the SCF + G-CSF-enhanced brain repair in TgNotch3R90C mouse model of CADASIL through the molecular, neurovascular structure and neurobehavioral approaches. It remains to be determined whether the SCF + G-CSF-increased cerebrovascular density would lead to an increase of cerebral blood flow in TgNotch3R90C mice and whether the SCF + G-CSF-increased dendritic and axonal density, and synaptic density in TgNotch3R90C mice would result in enhanced neural network functioning by electrophysiology.

5. Conclusions

Cerebral vasculature stability is crucially involved in brain health. The reductions of cerebral VEGF/VEGF-A and cerebral vasculature play a key pathological role in the development of CADASIL. Targeting prevention of cerebral vessel regression would be a novel therapeutic

strategy for delaying CADASIL progression. This mechanistic study provides evidence showing that SCF + G-CSF-enhanced brain repair in TgNotch3R90C mice is mediated through VEGF-A-regulated cerebrovascular regeneration. The findings of this study shed light on how hematopoietic growth factors, SCF + G-CSF, restrict the pathological progression of CADASIL.

Supplementary data to this article can be found online at https://doi.org/10.1016/j.nbd.2019.104561.

Acknowledgments

This work was supported by American Heart Association (15GRNT25700284). We thank Sandra McGillis for her assistance with proofreading.

References

Ambrose, C.T., 2017. Pro-angiogenesis therapy and aging: a mini-review. Gerontology 63 (5), 393–400.
Andreoli, C.M., Miller, J.W., 2007. Anti-vascular endothelial growth factor therapy for ocular neovascular disease. Curr. Opin. Ophthalmol. 18 (6), 502–508.
Badre, D., Kayser, A.S., et al., 2010. Frontal cortex and the discovery of abstract action rules. Neuron 66 (2), 315–326.
Baudrimont, M., Dubas, F., et al., 1993. Autosomal dominant leukoencephalopathy and subcortical ischemic stroke. A clinicopathological study. Stroke 24 (1), 122–125.
Bereczki, E., Branca, R.M., et al., 2018. Synaptic markers of cognitive decline in neurodegenerative diseases: a proteomic approach. Brain 141 (2), 582–595.
Betz, C., Lenard, A., et al., 2016. Cell behaviors and dynamics during angiogenesis. Development 143 (13), 2249–2260.
Brown, J.P., Couillard-Despres, S., et al., 2003. Transient expression of doublecortin during adult neurogenesis. J. Comp. Neurol. 467 (1), 1–10.
Brown, C.E., Li, P., et al., 2007. Extensive turnover of dendritic spines and vascular remodeling in cortical tissues recovering from stroke. J. Neurosci. 27 (15), 4101–4109.
Campolo, J., De Maria, R., et al., 2012. Impaired vasoreactivity in mildly disabled CADASIL patients. J. Neurol. Neurosurg. Psychiatry 83 (3), 268–274.
Cao, L., Jiao, X., et al., 2004. VEGF links hippocampal activity with neurogenesis, learning and memory. Nat. Genet. 36 (8), 827–835.
Chabriat, H., Bousser, M.G., et al., 1995. Cerebral autosomal dominant arteriopathy with subcortical infarcts and leukoencephalopathy: a positron emission tomography study in two affected family members. Stroke 26 (9), 1729–1730.
Chabriat, H., Pappata, S., et al., 2000. Cerebral hemodynamics in CADASIL before and after acetazolamide challenge assessed with MRI bolus tracking. Stroke 31 (8), 1904–1912.
Chabriat, H., Joutel, A., et al., 2009. Cadasil. Lancet Neurol. 8 (7), 643–653.
Chen, S.H., Yeh, C.H., et al., 2010. Premarin improves outcomes of spinal cord injury in male rats through stimulating both angiogenesis and neurogenesis. Crit. Care Med. 38 (10), 2043–2051.
Chen, Q., Zhang, H., et al., 2016. Endothelial cells are progenitors of cardiac pericytes and vascular smooth muscle cells. Nat. Commun. 7, 12422.
Cui, L., Duchamp, N.S., et al., 2015. NF-kappaB is involved in brain repair by stem cell factor and granulocyte-colony stimulating factor in chronic stroke. Exp. Neurol. 263, 17–27.
Cui, L., Wang, D., et al., 2016. Repairing the brain by SCF + G-CSF treatment at 6 months Postexperimental stroke: mechanistic determination of the causal link between neurovascular regeneration and motor functional recovery. ASN Neuro 8 (4).
De Guio, F., Vignaud, A., et al., 2014. Loss of venous integrity in cerebral small vessel disease: a 7-T MRI study in cerebral autosomal-dominant arteriopathy with subcortical infarcts and leukoencephalopathy (CADASIL). Stroke 45 (7), 2124–2126.
Dehmelt, L., Halpain, S., 2005. The MAP2/tau family of microtubule-associated proteins. Genome Biol. 6 (1), 204.
Di Donato, I., Bianchi, S., et al., 2017. Cerebral autosomal dominant Arteriopathy with subcortical infarcts and leukoencephalopathy (CADASIL) as a model of small vessel disease: update on clinical, diagnostic, and management aspects. BMC Med. 15 (1), 41.
Drachman, D.A., Smith, T.W., et al., 2017. Microvascular changes in down syndrome with Alzheimer's-type pathology: insights into a potential vascular mechanism for down syndrome and Alzheimer's disease. Alzheimers Dement. 13 (12), 1389–1396.
Dubroca, C., Lacombe, P., et al., 2005. Impaired vascular mechanotransduction in a transgenic mouse model of CADASIL arteriopathy. Stroke 36 (1), 113–117.
Dum, R.P., Levinthal, D.J., et al., 2016. Motor, cognitive, and affective areas of the cerebral cortex influence the adrenal medulla. Proc. Natl. Acad. Sci. U. S. A. 113 (35), 9922–9927.
Dziewulska, D., Lewandowska, E., 2012. Pericytes as a new target for pathological processes in CADASIL. Neuropathology 32 (5), 515–521.
Eilken, H.M., Dieguez-Hurtado, R., et al., 2017. Pericytes regulate VEGF-induced endothelial sprouting through VEGFR1. Nat. Commun. 8 (1), 1574.
Euston, D.R., Gruber, A.J., et al., 2012. The role of medial prefrontal cortex in memory and decision making. Neuron 76 (6), 1057–1070.
Feng, F., Cheng, Y., et al., 2014. Bevacizumab treatment reduces retinal neovascularization in a mouse model of retinopathy of prematurity. Int J Ophthalmol 7 (4), 608–613.
Ferrara, N., Gerber, H.-P., et al., 2003. The biology of VEGF and its receptors. Nat. Med. 9 (6), 669.
Flieger, D., Hainke, S., et al., 2006. Dramatic improvement in hereditary hemorrhagic telangiectasia after treatment with the vascular endothelial growth factor (VEGF) antagonist bevacizumab. Ann. Hematol. 85 (9), 631–632.
Fouda, A.Y., Alhusban, A., et al., 2017. Brain-derived neurotrophic factor knockdown blocks the Angiogenic and protective effects of angiotensin modulation after experimental stroke. Mol. Neurobiol. 54 (1), 661–670.
Ghosh, M., Balbi, M., et al., 2015. Pericytes are involved in the pathogenesis of cerebral autosomal dominant arteriopathy with subcortical infarcts and leukoencephalopathy. Ann. Neurol. 78 (6), 887–900.
Gleeson, J.G., Lin, P.T., et al., 1999. Doublecortin is a microtubule-associated protein and is expressed widely by migrating neurons. Neuron 23 (2), 257–271.
Gu, X., Liu, X.Y., et al., 2012. Ultrastructural changes in cerebral capillary pericytes in aged Notch3 mutant transgenic mice. Ultrastruct. Pathol. 36 (1), 48–55.
Herran, E., Perez-Gonzalez, R., et al., 2015. Enhanced hippocampal neurogenesis in APP/Ps1 mouse model of Alzheimer's disease after implantation of VEGF-loaded PLGA Nanospheres. Curr. Alzheimer Res. 12 (10), 932–940.
Holtmaat, A., Wilbrecht, L., et al., 2006. Experience-dependent and cell-type-specific spine growth in the neocortex. Nature 441 (7096), 979–983.
Hunt, C.A., Schenker, L.J., et al., 1996. PSD-95 is associated with the postsynaptic density and not with the presynaptic membrane at forebrain synapses. J. Neurosci. 16 (4), 1380–1388.
Jiang, X., Engelbach, J.A., et al., 2014. Anti-VEGF antibodies mitigate the development of radiation necrosis in mouse brain. Clin. Cancer Res. 20 (10), 2695–2702.
Jin, Q., Cheng, J., et al., 2014. Improvement of functional recovery by chronic metformin treatment is associated with enhanced alternative activation of microglia/macrophages and increased angiogenesis and neurogenesis following experimental stroke. Brain Behav. Immun. 40, 131–142.
Johnson, G.V., Jope, R.S., 1992. The role of microtubule-associated protein 2 (MAP-2) in neuronal growth, plasticity, and degeneration. J. Neurosci. Res. 33 (4), 505–512.
Joutel, A., 2011. Pathogenesis of CADASIL: transgenic and knock-out mice to probe function and dysfunction of the mutated gene, Notch3, in the cerebrovasculature. Bioessays 33 (1), 73–80.
Joutel, A., 2015. The NOTCH3ECD cascade hypothesis of cerebral autosomal-dominant arteriopathy with subcortical infarcts and leukoencephalopathy disease. Neurology and Clinical Neuroscience 3 (1), 1–6.
Joutel, A., Corpechot, C., et al., 1996. Notch3 mutations in CADASIL, a hereditary adult-onset condition causing stroke and dementia. Nature 383 (6602), 707–710.
Joutel, A., Andreux, F., et al., 2000. The ectodomain of the Notch3 receptor accumulates within the cerebrovasculature of CADASIL patients. J. Clin. Invest. 105 (5), 597–605.
Joutel, A., Monet, M., et al., 2004. Pathogenic mutations associated with cerebral autosomal dominant arteriopathy with subcortical infarcts and leukoencephalopathy differently affect Jagged1 binding and Notch3 activity via the RBP/JK signaling pathway. Am. J. Hum. Genet. 74 (2), 338–347.
Joutel, A., Monet-Lepretre, M., et al., 2010. Cerebrovascular dysfunction and microcirculation rarefaction precede white matter lesions in a mouse genetic model of cerebral ischemic small vessel disease. J. Clin. Invest. 120 (2), 433–445.
Kalimo, H., Viitanen, M., et al., 1999. CADASIL: hereditary disease of arteries causing brain infarcts and dementia. Neuropathol. Appl. Neurobiol. 25 (4), 257–265.
Karlsson, W.K., Sorensen, C.G., et al., 2017. l-Arginine and l-NMMA for assessing cerebral endothelial dysfunction in ischaemic cerebrovascular disease: a systematic review. Clin. Exp. Pharmacol. Physiol. 44 (1), 13–20.
Karlstrom, H., Beatus, P., et al., 2002. A CADASIL-mutated notch 3 receptor exhibits impaired intracellular trafficking and maturation but normal ligand-induced signaling. Proc. Natl. Acad. Sci. U. S. A. 99 (26), 17119–17124.
Kawada, H., Takizawa, S., et al., 2006. Administration of hematopoietic cytokines in the subacute phase after cerebral infarction is effective for functional recovery facilitating proliferation of intrinsic neural stem/progenitor cells and transition of bone marrow-derived neuronal cells. Circulation 113 (5), 701–710.
Kida, H., Tsuda, Y., et al., 2016. Motor training promotes both synaptic and intrinsic plasticity of layer II/III pyramidal neurons in the primary motor cortex. Cereb. Cortex 26 (8), 3494–3507.
Kiriakidis, S., Andreakos, E., et al., 2003. VEGF expression in human macrophages is NF-kappaB-dependent: studies using adenoviruses expressing the endogenous NF-kappaB inhibitor IkappaBalpha and a kinase-defective form of the IkappaB kinase 2. J. Cell Sci. 116 (Pt 4), 665–674.
Lacombe, P., Oligo, C., et al., 2005. Impaired cerebral vasoreactivity in a transgenic mouse model of cerebral autosomal dominant arteriopathy with subcortical infarcts and leukoencephalopathy arteriopathy. Stroke 36 (5), 1053–1058.
Laske, C., Stellos, K., et al., 2008. Decreased plasma and cerebrospinal fluid levels of stem cell factor in patients with early Alzheimer's disease. J. Alzheimers Dis. 15 (3), 451–460.
Laske, C., Stellos, K., et al., 2009. Decreased plasma levels of granulocyte-colony stimulating factor (G-CSF) in patients with early Alzheimer's disease. J. Alzheimers Dis. 17 (1), 115–123.
Lazarini, F., Lledo, P.M., 2011. Is adult neurogenesis essential for olfaction? Trends Neurosci. 34 (1), 20–30.
Lieberwirth, C., Pan, Y., et al., 2016. Hippocampal adult neurogenesis: its regulation and potential role in spatial learning and memory. Brain Res. 1644, 127–140.
Liu, X.Y., Gonzalez-Toledo, M.E., et al., 2015. Stem cell factor and granulocyte colony-stimulating factor exhibit therapeutic effects in a mouse model of CADASIL. Neurobiol. Dis. 73, 189–203.
Low, W.C., Santa, Y., et al., 2006. CADASIL-causing mutations do not alter Notch3 receptor processing and activation. Neuroreport 17 (10), 945–949.

Lu, D., Goussev, A., et al., 2004. Atorvastatin reduces neurological deficit and increases synaptogenesis, angiogenesis, and neuronal survival in rats subjected to traumatic brain injury. J. Neurotrauma 21 (1), 21–32.
Luo, H., Hasegawa, K., et al., 2017. Comparison of the upper marginal neurons of cortical layer 2 with layer 2/3 pyramidal neurons in mouse temporal cortex. Front. Neuroanat. 11, 115.
Ma, L., Qiao, Q., et al., 2016. Experience-dependent plasticity of dendritic spines of layer 2/3 pyramidal neurons in the mouse cortex. Dev Neurobiol 76 (3), 277–286.
Madelaine, R., Sloan, S.A., et al., 2017. MicroRNA-9 couples brain neurogenesis and angiogenesis. Cell Rep. 20 (7), 1533–1542.
Maguire, E.A., Gadian, D.G., et al., 2000. Navigation-related structural change in the hippocampi of taxi drivers. Proc. Natl. Acad. Sci. U. S. A. 97 (8), 4398–4403.
Masek, J., Andersson, E.R., 2017. The developmental biology of genetic notch disorders. Development 144 (10), 1743–1763.
Miao, Q., Paloneva, T., et al., 2004. Fibrosis and stenosis of the long penetrating cerebral arteries: the cause of the white matter pathology in cerebral autosomal dominant arteriopathy with subcortical infarcts and leukoencephalopathy. Brain Pathol. 14 (4), 358–364.
Miao, Q., Paloneva, T., et al., 2006. Arterioles of the lenticular nucleus in CADASIL. Stroke 37 (9), 2242–2247.
Mitchell, A., Adams, L.A., et al., 2008. Bevacizumab reverses need for liver transplantation in hereditary hemorrhagic telangiectasia. Liver Transpl. 14 (2), 210–213.
Monet, M., Domenga, V., et al., 2007. The archetypal R90C CADASIL-NOTCH3 mutation retains NOTCH3 function in vivo. Hum. Mol. Genet. 16 (8), 982–992.
Monet-Lepretre, M., Bardot, B., et al., 2009. Distinct phenotypic and functional features of CADASIL mutations in the Notch3 ligand binding domain. Brain 132 (Pt 6), 1601–1612.
Navone, S.E., Marfia, G., et al., 2013. Isolation and expansion of human and mouse brain microvascular endothelial cells. Nat. Protoc. 8 (9), 1680–1693.
Peters, N., Herzog, J., et al., 2004a. A two-year clinical follow-up study in 80 CADASIL subjects: progression patterns and implications for clinical trials. Stroke 35 (7), 1603–1608.
Peters, N., Opherk, C., et al., 2004b. CADASIL-associated Notch3 mutations have differential effects both on ligand binding and ligand-induced Notch3 receptor signaling through RBP-Jk. Exp. Cell Res. 299 (2), 454–464.
Peters, N., Freilinger, T., et al., 2008. Enhanced L-arginine-induced vasoreactivity suggests endothelial dysfunction in CADASIL. J. Neurol. 255 (8), 1203–1208.
Phillips, A.A., Chan, F.H., et al., 2016. Neurovascular coupling in humans: physiology, methodological advances and clinical implications. J. Cereb. Blood Flow Metab. 36 (4), 647–664.
Ping, S., Qiu, X., et al., 2018. Stem cell factor in combination with granulocyte colony-stimulating factor reduces cerebral capillary thrombosis in a mouse model of CADASIL. Cell Transplant. 27 (4), 637–647.
Robinson, J.L., Molina-Porcel, L., et al., 2014. Perforant path synaptic loss correlates with cognitive impairment and Alzheimer's disease in the oldest-old. Brain 137 (Pt 9), 2578–2587.
Rosenstein, J.M., Mani, N., et al., 1998. Patterns of brain angiogenesis after vascular endothelial growth factor administration in vitro and in vivo. Proc. Natl. Acad. Sci. U. S. A. 95 (12), 7086–7091.
Ruan, L., Wang, B., et al., 2015. Coupling of neurogenesis and angiogenesis after ischemic stroke. Brain Res. 1623, 166–173.
Ruchoux, M.M., Domenga, V., et al., 2003. Transgenic mice expressing mutant Notch3 develop vascular alterations characteristic of cerebral autosomal dominant arteriopathy with subcortical infarcts and leukoencephalopathy. Am. J. Pathol. 162 (1), 329–342.
Ruck, T., Bittner, S., et al., 2014. Isolation of primary murine brain microvascular endothelial cells. J. Vis. Exp. 93, e52204.
Rutten, J.W., Dauwerse, H.G., et al., 2016. Archetypal NOTCH3 mutations frequent in public exome: implications for CADASIL. Ann Clin Transl Neurol 3 (11), 844–853.
Ryu, J.K., Cho, T., et al., 2009. Microglial VEGF receptor response is an integral chemotactic component in Alzheimer's disease pathology. J. Neurosci. 29 (1), 3–13.
Shibuya, M., 2009. Brain angiogenesis in developmental and pathological processes: therapeutic aspects of vascular endothelial growth factor. FEBS J. 276 (17), 4636–4643.
Smith, J.D., Davies, N., et al., 2001. Cyclic stretch induces the expression of vascular endothelial growth factor in vascular smooth muscle cells. Endothelium 8 (1), 41–48.
Stoltz, R.A., Abraham, N.G., et al., 1996. The role of NF-kappaB in the angiogenic response of coronary microvessel endothelial cells. Proc. Natl. Acad. Sci. U. S. A. 93 (7), 2832–2837.
Sweeney, M.D., Ayyadurai, S., et al., 2016. Pericytes of the neurovascular unit: key functions and signaling pathways. Nat. Neurosci. 19 (6), 771–783.
Talwar, T., Srivastava, M.V., 2014. Role of vascular endothelial growth factor and other growth factors in post-stroke recovery. Ann. Indian Acad. Neurol. 17 (1), 1–6.
Tjia, M., Yu, X., et al., 2017. Pyramidal neurons in different cortical layers exhibit distinct dynamics and plasticity of apical dendritic spines. Front Neural Circuits 11, 43.
Tuominen, S., Miao, Q., et al., 2004. Positron emission tomography examination of cerebral blood flow and glucose metabolism in young CADASIL patients. Stroke 35 (5), 1063–1067.
Ulfig, N., Nickel, J., et al., 1998. Monoclonal antibodies SMI 311 and SMI 312 as tools to investigate the maturation of nerve cells and axonal patterns in human fetal brain. Cell Tissue Res. 291 (3), 433–443.
Valley, M.T., Mullen, T.R., et al., 2009. Ablation of mouse adult neurogenesis alters olfactory bulb structure and olfactory fear conditioning. Front. Neurosci. 3, 51.
Vallon, M., Chang, J., et al., 2014. Developmental and pathological angiogenesis in the central nervous system. Cell. Mol. Life Sci. 71 (18), 3489–3506.
Venkat, P., Chopp, M., et al., 2016. New insights into coupling and uncoupling of cerebral blood flow and metabolism in the brain. Croat Med J 57 (3), 223–228.
Villa, N., Walker, L., et al., 2001. Vascular expression of notch pathway receptors and ligands is restricted to arterial vessels. Mech. Dev. 108 (1–2), 161–164.
Volz, K.S., Jacobs, A.H., et al., 2015. Pericytes are progenitors for coronary artery smooth muscle. Elife 4.
Welte, K., Platzer, E., et al., 1985. Purification and biochemical characterization of human pluripotent hematopoietic colony-stimulating factor. Proc. Natl. Acad. Sci. U. S. A. 82 (5), 1526–1530.
Welti, J., Loges, S., et al., 2013. Recent molecular discoveries in angiogenesis and antiangiogenic therapies in cancer. J. Clin. Invest. 123 (8), 3190–3200.
Wiedenmann, B., Franke, W.W., et al., 1986. Synaptophysin: a marker protein for neuroendocrine cells and neoplasms. Proc. Natl. Acad. Sci. U. S. A. 83 (10), 3500–3504.
Williamson, W., Lewandowski, A.J., et al., 2018. Association of Cardiovascular Risk Factors with MRI indices of cerebrovascular structure and function and white matter Hyperintensities in young adults. Jama 320 (7), 665–673.
Xu, T., Yu, X., et al., 2009. Rapid formation and selective stabilization of synapses for enduring motor memories. Nature 462 (7275), 915–919.
Yang, G., Pan, F., et al., 2009. Stably maintained dendritic spines are associated with lifelong memories. Nature 462 (7275), 920–924.
Yang, K., Banerjee, S., et al., 2013. Regulation of pre-natal circle of Willis assembly by vascular smooth muscle Notch signaling. Dev. Biol. 381 (1), 107–120.
Zhao, L.R., Berra, H.H., et al., 2007. Beneficial effects of hematopoietic growth factor therapy in chronic ischemic stroke in rats. Stroke 38 (10), 2804–2811.
Zlokovic, B.V., 2005. Neurovascular mechanisms of Alzheimer's neurodegeneration. Trends Neurosci. 28 (4), 202–208.
Zsebo, K.M., Wypych, J., et al., 1990. Identification, purification, and biological characterization of hematopoietic stem cell factor from buffalo rat liver–conditioned medium. Cell 63 (1), 195–201.